CatSperζ Regulates the Structural Continuity of Sperm Ca^{2+} Signaling Domains and is Required for Normal Fertility

Jean-Ju Chung[1,2,4*], Kiyoshi Miki[1], Doory Kim[3], Sang-Hee Shim[3,6], Huanan F. Shi[4], Jae Yeon Hwang[4], Xinjiang Cai[5], Yusuf Iseri[1], Xiaowei Zhuang[3], David E. Clapham[1,2*]

[1]Howard Hughes Medical Institute, Boston Children's Hospital, Boston, Massachusetts, 02115, USA.
[2]Department of Neurobiology, Harvard Medical School, Boston, Massachusetts 02115, USA.
[3]Howard Hughes Medical Institute, Department of Chemistry and Chemical Biology, Department of Physics, Harvard University, Cambridge, Massachusetts 02138, USA.
[4]Department of Cellular & Molecular Physiology, Yale School of Medicine, New Haven, Connecticut 06520, USA.
[5]Department of Medicine, Icahn School of Medicine at Mount Sinai, New York, NY, 10468, USA.

*Correspondence: jean-ju.chung@yale.edu (J.-J.C.), dclapham@enders.tch.harvard.edu (D.E.C.)
[6]Present address: Department of Chemistry, Korea University, Seoul, 02481, Republic of Korea

Key words: mammalian fertilization; sperm motility; sperm ion channels; sperm rheotaxis; Ca^{2+} signaling domains; super-resolution imaging

Abstract

We report that the *Gm7068* (*CatSperε*) and *Tex40* (*CatSperζ*) genes encode novel subunits of a 9-subunit CatSper ion channel complex. Targeted disruption of *CatSperζ* reduces CatSper current and sperm rheotactic efficiency in mice, resulting in severe male subfertility. Normally distributed in linear quadrilateral nanodomains along the flagellum, the complex lacking CatSperζ is disrupted at ~0.8 µm intervals along the flagellum. This disruption renders the proximal flagellum inflexible and alters the 3D flagellar envelope, thus preventing sperm from reorienting against fluid flow *in vitro* and efficiently migrating *in vivo.* Ejaculated *CatSperζ*-null sperm cells retrieved from the mated female uterus partially rescue *in vitro* fertilization (IVF) that failed with epididymal spermatozoa alone. Human CatSperε is quadrilaterally arranged along the flagella, similar to the CatSper complex in mouse sperm. We speculate that the newly identified CatSperζ subunit is a late evolutionary adaptation to maximize fertilization inside the mammalian female reproductive tract.

Introduction

Sperm hyperactivation, characterized by a large asymmetric lateral displacement of the flagellum (Ishijima et al., 2002), is required for normal mammalian sperm navigation (Demott and Suarez, 1992), rheotaxis (Miki and Clapham, 2013), and *zona pellucida* (ZP) penetration (Stauss et al., 1995). Calcium influx through the flagellar Ca^{2+} ion channel, CatSper, triggers hyperactivation (Carlson et al., 2003; Kirichok et al., 2006; Ren et al., 2001) and leads to changes in the flagellar envelope during capacitation (Chung et al., 2011; Quill et al., 2003). In hyperactivated spermatozoa, the transverse flagellar force is larger than the propulsive flagellar force due to the increase in mid-piece curvature (α angle), which enables a larger range of motion and typical figure-of-eight swimming trajectories compared to the nearly straight paths of non-hyperactivated spermatozoa (Ishijima, 2011). Transverse force facilitates sperm penetration through the cumulus and ZP (Ishijima, 2011; Yanagimachi, 1966). Spermatozoa from all *CatSper*-null *(1-4* or *δ)* males have smaller α angles than wt spermatozoa upon capacitation (Chung et al., 2011; Qi et al., 2007). Consistently, *CatSper*-null mutant spermatozoa migrate inefficiently *in vivo* (Chung et al., 2014; Ho et al., 2009) and fail to penetrate the ZP (Ren et al., 2001).

Sperm rheotax against Fallopian tubular and isthmus fluid flow (Miki and Clapham, 2013). Rheotactic turning to reorient to directional flow depends on flagellar rolling, not the sperm head or its geometry, as demonstrated by the rheotaxis of headless mouse sperm (Miki and Clapham, 2013). CatSper channels form unique Ca^{2+} signaling domains in linearly quadrilateral arrays along the principal piece of sperm flagella. The integrity of these domains is necessary to time and/or maintain hyperactivated motility (Chung et al., 2014). Thus, *CatSper1*-null sperm cannot rheotax due to defects in rolling (Miki and Clapham, 2013), and presumably exert less lateral force in escaping from epithelial walls (Ho et al., 2009) or in pushing cumulus cells aside. In general, however, there is a lack of understanding of the steps between CatSper-mediated calcium entry, Ca^{2+}-modified phosphorylation cascades, and the resulting structural changes underlying orchestrated flagellar movement.

Here, we reveal that the murine *Gm7068* (*C1orf101-like)* and *Tex40* genes encode two new subunits of the CatSper ion channel complex, CatSper ε and ζ, respectively. In this study, we focus primarily on CatSperζ's function. Genetic disruption of mammalian-specific CatSperζ reduces CatSper current in the sperm flagellum and hyperactivated motility, resulting in severe subfertility. We use high speed video microscopy and digital image analysis to determine swimming trajectory and flagellar waveform in detail. Surprisingly, abrogation of CatSperζ renders the proximal flagellum inflexible but preserves overall motility, thus resulting in restriction of the 3D flagellar envelope, inefficient sperm rheotaxis *in vitro,* and delayed sperm migration *in vivo*. Using super-resolution microscopy, we demonstrated that the structurally distinct CatSper Ca^{2+} signaling domains along the flagellum (Chung et al., 2014) becomes fragmented in the absence of *CatSperζ*. We demonstrate that IVF failure of *CatSperζ*-null spermatozoa is partially rescued by using ejaculated sperm recovered from the uterus of mated females, explaining the discrepancy between *in vitro* and *in vivo* fertilizing ability. Finally, we show that mouse and human spermatozoa have similar macroscopic organization of the CatSper complex.

Results

CatSper ε and ζ: Two New Accessory Proteins in the CatSper Channel Complex

We previously identified seven protein components of the CatSper channel complex (CatSper1-4, β, γ, and δ) from mouse testis using tandem affinity purification (Chung et al., 2011). As the most biochemically complex ion channel known to date, it has not been possible to express functional CatSper

channels in heterologous systems. This includes many attempts in many cell types, including simultaneous injection of all 7 CatSper mRNAs into *Xenopus* oocytes (*data not shown*). Therefore, we continued to seek potential additional components to more thoroughly understand CatSper channel assembly and trafficking. We identified a mouse homolog of human *C1orf101* (*C1orf101-like*, currently *Gm7068*) (**Figure 1A)** based on its sequence homology to the C-terminal extracellular domain of CatSperδ (**Figure 1-figure supplement 1A**). This testis-specific gene (**Figure 1-figure supplement 2A**) is predicted to encode a single transmembrane (TM) protein (**Figure 1C** and **Figure 1-figure supplements 1B, C**). In addition, a small soluble protein encoded by another testis-specific gene, *Tex40* (**Figure 1-figure supplement 2A**), was found to be associated with the CatSper channel complex (**Figures 1B, 1C,** and **Figure 1-figure supplement 1D**). In this study, we refer to the *C1orf101-like* and *Tex40* genes as *CatSperε* and *CatSperζ*, respectively (see Molecular Cloning, **Materials and Methods**). Like the other CatSper accessory subunits (Chung et al., 2011), both *CatSperε* and *CatSperζ* mRNAs express specifically in germ cells and are detected before *CatSper1* expression during postnatal development (**Figure 1-figure supplements 2B, C**). Moreover, mouse CatSper ε and ζ proteins partition into the testis microsome fraction (P) (**Figure 1-figure supplement 2D)**, complex with CatSper1, and exhibit interdependence with expression of the other CatSper subunits (**Figures 1D-1F**). In both human and mouse sperm cells, CatSper ε and ζ proteins are localized to the principal piece of the tails (**Figures 1G, 1H** and **Figure 1-figure supplements 2E-G**).

CatSper ε and ζ Localize at Quadrilateral Ca^{2+} Signaling Domains in Sperm Flagella.

Mouse CatSper proteins form a unique pattern of four linear ('racing stripes') Ca^{2+} signaling domains running down the four quadrants of the principal piece of the flagellum (Chung et al., 2014). We examined whether ε and ζ share this distinctive compartmentalization. The antibodies, anti-hε31, recognizing the N-terminal extracellular region of human CatSperε, and anti-mζ174, against the very C-terminus of mouse CatSperζ, were suitable for 3D stochastic optical reconstruction microscopy (STORM) (**Figures 1F-1H** and **Figure 1-figure supplement 2E**). CatSperζ and CatSperε show the apparent 4-fold arrangement of CatSper1, β and δ subunits in mouse (**Figure 1I**) and human (**Figure 1J**) spermatozoa.

CatSperζ-null Male Mice Have Severely Impaired Fertility.

The lack of functional expression of CatSper channels in heterologous systems requires that genetic manipulation be used to study the function of each component. *CatSperε* has the same ancient origin at the root of early eukaryotic evolution as those of *CatSpers1-4*, *β*, and *γ* and the same pattern of extensive lineage-specific gene loss as *β* and *γ* through metazoan evolution (**Figure 2-figure supplement 1A**) (Cai et al., 2014). While CatSper δ and ε share high C-terminal sequence homology (**Figure 1-figure supplement 1A**), CatSperδ appears later in evolution (**Figure 2-figure supplement 1A**). In contrast, CatSperζ has no conserved domains and, like hyperactivated motility, is only present in mammals (**Figure 2-figure supplement 1A**), leading us to speculate that CatSperζ is a required evolutionary adaptation to mammalian fertilization. Based on sequence homology and conservation, we anticipated that deletion of CatSperε would likely be the same as the existing knockout of other CatSper subunits, but deletion of CatSperζ might provide new insights into spermatozoan adaptations to changes concomitant with the evolution of mammalian fertilization. To test this idea, we began by generating a *CatSperζ*-null mouse line from *Tex40* gene targeted ES cell clones. *Tex40* is a small gene composed of 5 exons that spans only ~ 3 kb on chromosome 11 (**Figure 2-figure supplement 1B**). Deletion of exons 2-4 was confirmed in the homozygous null mouse (**Figure 2-figure supplement 1C**). No CatSperζ protein was detected in *Tex40*-null spermatozoa by immunoblotting and immunocytochemistry (**Figure 2-figure supplement 1D, E**).

CatSperζ-null mutant mice are indistinguishable from their wt or heterozygous (het) littermates in appearance, gross behavior, or survival. In addition, no morphological differences were observed by histological examination of testis and epididymis (*data not shown*). Sperm morphology and epididymal sperm number from *CatSperζ*-null mice were not significantly different from those of 2-3 month old paired heterozygous littermates (**Figure 2-figure supplement 1E** and **Figure 2-figure supplement 2A**). *CatSperζ*-null female mice exhibited normal mating behavior and gave birth to litters comparable to those of het females when mated with wt or het males (**Figure 2-figure supplement 2B**). However, when *CatSperζ*-null male mice were mated with wt or het females, they were severely subfertile: 20% (5/25) *CatSperζ*-null males were completely infertile over 6 months (**Figure 2A**), and progeny of the fertile paternal *CatSperζ*-null mice were significantly fewer in number (**Figures 2B** and **Figure 2-figure supplement 2B**). The latency from pair formation to birth of these offspring from *ζ*-null males was ≥ 10 days compared to those from wt or het males (*data not shown*).

We examined the number of sperm within cumulus oocyte complexes (COCs) after copulation and checked *in vivo* fertilization rates by isolating the COCs and/or embryos from the female ampullae. At 8 h after coitus, no sperm was found in the COCs when mated with *CatSperζ*-null male mice (**Figure 2C**). In contrast, the majority of the COCs from *CatSperζ*-het mated females had one or more sperm cells within the complex. When mated with *CatSperζ*-het males, more 2-cell eggs were observed over time after coitus, while the fertilization rate by *CatSperζ*-null males did not change significantly (**Figures 2D** and **Figure 2-figure supplement 2C**). These data suggest that *CatSperζ*-null sperm migration is delayed in the female reproductive tract.

CatSperζ-null sperm cells have rigid proximal flagella.

To understand why *CatSperζ*-null spermatozoa did not efficiently migrate in the female reproductive tract, we first investigated sperm motility using computer assisted sperm analysis (CASA) (**Figure 2-figure supplement 2D**). The percentage of motile spermatozoa was not significantly different and most motility parameters of *ζ*-null spermatozoa were comparable to those of *ζ*-het sperm cells. However, the characteristic increase of lateral head displacement upon capacitation was not observed in *ζ*-null spermatozoa (**Figure 2-figure supplement 2D**), suggesting that hyperactivated motility was reduced. Ninety minutes after capacitation, there was a less marked difference in swimming trajectories of *ζ*-null spermatozoa compared to *ζ*-het spermatozoa, supporting this notion (**Figure 2E** and **Movie S1**). Further analysis of flagellar amplitude and waveforms of tethered spermatozoa revealed a striking rigidity of *ζ*-null spermatozoa from their midpiece to midway down the principal piece (**Figure 2F** and **Movie S2**). This phenotype was also observed from hyperactivation-deficient *CatSper2*-null patients (Smith et al., 2013). After incubation under capacitating conditions for 90 min, we observed that *ζ*-null spermatozoa beat only at the very distal end of a flagellum (**Movie S3**). Moreover, *CatSperζ*-null spermatozoa remain bent in the anti-hook direction (Ishijima et al., 2002)(**Figure 2F**, **Movies S2** and **S3**). The anti-hook bend predominates as the pro-hook bend (initiated by the CatSper-mediated Ca^{2+} signaling pathway (Chang and Suarez, 2011) is dysregulated in *CatSperζ*-null spermatozoa.

Reduced CatSper Current in *CatSperζ*-null Spermatozoa.

To examine how Ca^{2+} signaling in *CatSperζ*-null spermatozoa is impaired, we first examined $I_{CatSper}$, the sperm-specific Ca^{2+}-selective ion current. Since Ca^{2+} has high affinity to calcium-selective pores (Almers et al., 1984), CatSper permeation of monovalents increases when external calcium is removed (Kirichok et al., 2006; Navarro et al., 2007). In divalent-free (DVF) solutions, wt spermatozoan $I_{CatSper}$ conducts a large Na^{+} current, which is completely absent in mice lacking *CatSpers1, 2, 3, 4*, or *δ*(Chung et al., 2011; Kirichok et al., 2006; Qi et al., 2007). However, in *CatSperζ*-null spermatozoa, monovalent CatSper current is present but reduced to ~60% of normal (-426 ± 50 pA at -100 mV; **Figure 3A**) compared to

control *CatSperζ*-het spermatozoa (-683 ± 77 pA at -100 mV; **Figure 3B**). Thus, in the absence of CatSperζ, the CatSper channel complex is still targeted to the flagellar membrane and forms functional channels. We hypothesize that the reduction in CatSper current reflected decreased protein expression levels.

P2X receptors are nonselective ion channels gated by purines such as ATP. The ATP-activated cation-nonselective current in the midpiece of murine sperm is mediated by the P_2X_2 purinergic receptor (Navarro et al., 2011). In *CatSperζ*-null spermatozoa, I_{ATP} did not differ substantially from heterozygous spermatozoa (**Figures 3A** and **3B**), supporting the assumption that there is selective down regulation of CatSper channels. Smaller $I_{CatSper}$ explains, in part, the attenuated hyperactivated motility, delayed sperm migration, and male subfertility (**Figures 2A-2E**). Protein tyrosine phosphorylation (P-Tyr), a hallmark of sperm capacitation, is potentiated and delocalized in *CatSper* knockout mice (Chung et al., 2014) or when Ca^{2+} influx is pharmacologically blocked (Navarrete et al., 2015). Upon capacitation, P-Tyr was more prominent in *CatSperζ*-null spermatozoa than wt, but to a lesser extent than *CatSper1*-null spermatozoa (**Figure 2-figure supplement 2E**), consistent with the reduced calcium current. It is, however, also possible that an altered arrangement of the CatSper complex and/or its interaction with target proteins in the linear domains could have contributed to these functional deficits.

Abrogation of *CatSperζ* Retards Targeting of the CatSper Complex to Flagella.

To better understand why $I_{CatSper}$ is reduced in *CatSperζ-null* spermatozoa, we examined levels of protein expression in *CatSperζ*-null spermatozoa (**Figure 4A**). Expression of other CatSper subunits were detected in *CatSperζ*-null spermatozoa, albeit at 30-60% lower levels than that of wt (**Figure 4B**), consistent with reduced $I_{CatSper}$ (**Figure 3**). This contrasts with the complete absence of other CatSper subunits in *CatSper1*- and *CatSperδ*-null spermatozoa. mRNA and protein levels of other CatSper subunits were not reduced in the testis of *CatSperζ*-null mice (**Figures 4C** and **4D**), suggesting that the defect occurs during or after assembly of the protein complex.

CatSperζ Is Essential in Maintaining the Continuity of Linear Flagellar CatSper Ca^{2+} Domains.

Loss of *CatSperζ* resulted in fragmentation of CatSper1 staining on the flagellar membrane and these defects are large enough to be resolved by confocal imaging (**Figure 5A**). These gaps were not observed in wt/het (**Figures 1H** and **Figure 2-figure supplement 1E**) or previous wt and CatSper knockout studies (Chung et al., 2011; Chung et al., 2014; Liu et al., 2007; Ren et al., 2001). 3D STED and 3D STORM super-resolution microscopies clearly demonstrate that structural continuity is interrupted in *CatSperζ*-null spermatozoa - each 'stripe' of the CatSper domains is fragmented, while the overall quadrilateral structure is maintained (**Figures 5B** and **5C**). Cross-sections of the 3D STORM image of wt flagellum show the normal four tight clusters (**Figure 5C**, lower), represented as four lines in the 2D angular profiles of surface localizations (**Figure 5-figure supplement 1A, E;** inset) as previously observed (Chung et al., 2014). In *CatSperζ*-null spermatozoa, however, the four lines in the 2D angular profiles were interrupted (**Figure 5-figure supplement 1B**). To examine whether the interruptions were periodic, we performed autocorrelation analysis and Fourier transform of STORM images of *CatSperζ*-null sperm flagella (**Figure 5-figure supplement 1C-F**). Autocorrelation analysis of the *CatSperζ*-null sperm flagella exhibited enhanced periodicity compared to the wt flagellum, with the first peak at ~850 nm (**Figure 5-figure supplement 1C, D**). The Fourier transform shows a fundamental frequency of $(800\ nm)^{-1}$ (**Figure 5-figure supplement 1F**). We assume this thinning of one or more linear domains reflects an underlying structural periodicity that regulates CatSper complex trafficking or membrane insertion.

CatSperζ-null Spermatozoa Rheotax Inefficiently with Reduced Torque

Thus far, our results show that *CatSperζ*-null sperm have reduced $I_{CatSper}$, dysregulated structural continuity of the CatSper Ca^{2+} signaling domains, beat in an atypical pattern, and are delayed in migrating in the female reproductive tract, resulting in reduced male fertility. Rheotactic guidance for sperm over long distances requires rotational motion during CatSper-mediated hyperactivated motility (Miki and Clapham, 2013). We thus measured rheotactic parameters and the rotation rate of *CatSperζ*-null spermatozoa with a particular focus on whether their proximal tail rigidity and subsequent low amplitude lateral movement (**Figure 2**) affects sperm movement. In flow-directed capillary tubes (Miki and Clapham, 2013), we observed that the rheotactic ability of *CatSperζ*-null spermatozoa was significantly reduced (**Figures 6A, 6B** and **Figure 6-figure supplement 1A**). At all flow rates tested, most motile *CatSperζ*-null spermatozoa were unable reorient to swim against the flow and were swept out of the tube (**Movie S4**). In contrast, 85% of motile heterozygous spermatozoa displayed rheotactic behaviors by maintaining their position or swimming upstream for more than 2 s of the 9 s period of recording (**Figures 6B** and **Movie S4**).

We next examined rotational motion of *CatSperζ*-null spermatozoa. At high viscosities (0.3% methyl cellulose (MC), cP=6.7), uncapacitated *ζ*-het spermatozoa swim in circles (**Figure 6C**, left and **Movie S5**), while capacitated *ζ*-het spermatozoa swim in a more linear path as they rotate around a longitudinal axis, like wt spermatozoa (**Movie S6**) (Miki and Clapham, 2013). Interestingly, *ζ*-null spermatozoa exhibit linear migration as they can rotate along the tail axis regardless of capacitating conditions, even at higher viscosities (**Figure 6C**, right and **Movies S5** and **S6**). Indeed, uncapacitated *CatSperζ*-null spermatozoa rotate ~50% faster than *ζ*-het spermatozoa (**Figure 6D**). This indicates that *CatSperζ*-null spermatozoa have less lateral motion and are subject to less torque by the moving stream. Spatially, the spermatozoan traces out a less conical 3D envelope (**Figures 2F** and **Figure 6-figure supplement 1B**). In short, the rigidity of the *CatSperζ*-null sperm proximal tail constrains its motion to that of a propeller-driven rod.

Compromised Ca^{2+} Signaling Alters the Sperm's 3D Flagellar Envelope and Movement

We next examined the relation between external calcium entry and sperm function. First, we tested whether increasing extracellular [Ca^{2+}] could rescue *ζ*-null sperm motility. After incubation for 90 min with a 2-fold greater [Ca^{2+}], most *CatSperζ*-null sperm remain bent in the anti-hook orientation with a rigid proximal tail (**Figure 6-figure supplement 1C**, *ζ*(-/-) middle, and **Movie S8**). A few *ζ*-null spermatozoa partially recover, bending occasionally in the pro-hook direction with hyperactivated motility (**Figure 6-figure supplement 1C**, *ζ*(-/-) right, and **Movie S8**). Conversely, a 20-fold reduction of extracellular [Ca^{2+}] alone did not significantly alter the flagellar waveforms of *ζ*-het spermatozoa within 90 minutes (**Figure 6-figure supplement 1C** and **Movies S7** and **S8**).

A transient Ca^{2+} pulse induced by Ca^{2+} ionophore, A23187, significantly reduces the time required for wt sperm to develop hyperactivated motility (Tateno et al., 2013). Moreover, a short (10 min) exposure to A23187 can rescue defects in hyperactivated motility and the fertilizing capability of *CatSper1*-null sperm *in vitro* (Navarrete et al., 2016). We tested the relation of calcium transients to hyperactivated motility in *CatSper ζ*-het and null sperm. In *ζ*-het spermatozoa, an A23187-induced Ca^{2+} pulse followed by washout, enables full hyperactivation, characterized by wide lateral displacement with large midpiece α angle within 30 min (**Figure 6-figure supplement 1D** and **Movies S9** and **S10**). However, in *ζ*-null sperm, the same treatment improved the flexibility of the proximal flagella, particularly in the principal piece, but the midpiece remained largely inflexible (**Figure 6-figure supplement 1D** and **Movies S9** and **S10**). Building on our previous work, the present study suggests that calcium entry through CatSper channels has time-dependent, complex effects on the coordination of

motility and that loss of ζ results in reduced $I_{CatSper}$, changes in calcium signaling, and structural alterations of the flagellum.

CatSperζ-null Sperm Cells Inefficiently Penetrate the Egg Cumulus.

We performed *in vitro* fertilization (IVF) to determine how the low rotational torque generated by *CatSper*ζ-null spermatozoa affects sperm-egg interactions. We found that these spermatozoa cannot fertilize cumulus-intact oocytes (**Figure 6E**), but could dissociate the cumulus cell layers and bind to the ZP (*data not shown*). Cumulus removal did not change the fertilization rate of ZP intact oocytes by *CatSper*ζ-null spermatozoa. Furthermore, this rate that was only marginally enhanced by destabilization of the ZP by 2 mM glutathione (**Figure 6F**) (Miyata et al., 2015). This indicates that reduced hyperactivated motility alone does not explain the failure of *CatSper*ζ-null spermatozoa in IVF. One possibility is that the kinetics of capacitation *in vitro* is different from that *in vivo*, resulting from fluctuations in timing or amplitude of known factors (e.g., HCO_3, pH) or from unknown factors present in seminal and/or female fluids. We then compared IVF rates with ejaculated and epididymal spermatozoa of *CatSper*ζ-null mice. When ejaculated spermatozoa flushed from the uterus of the mated females were used in IVF trials, 20% of oocytes incubated with ζ-null spermatozoa developed into two-cell embryos (**Figure 6E**). This compares to 50% of oocytes incubated with ζ-het ejaculated (*data not shown*), or epididymal sperm. Thus, additional factors may be functionally relevant in *in vivo* fertilization.

Discussion

Complex Protein Composition and Conservation of Compartmentalization in Mammals.

Sperm hyperactivation and normal fertility in mammals requires the unique CatSper channel complex. With 4 distinct pore-forming gene products (CatSper 1-4) and, now, 5 accessory subunits (β, γ, δ, ε, and ζ), the CatSper channel is the most complex of known ion channels. This may reflect the relatively high evolutionary pressure on spermatozoan evolution (Swanson and Vacquier, 2002; Torgerson et al., 2002), and various adaptations to different modes of fertilization. Like many gamete-specific proteins and the other CatSper proteins reported so far (Cai and Clapham, 2008; Chung et al., 2011), mouse and human CatSper ε and ζ show signs of rapid evolutionary change with only 50 and 45% amino acid sequence identity, respectively. In particular, the sequence regions outside TM segments and the pore loop of CatSper proteins are poorly conserved across species, indicating these regions possibly convey species-specific modulation of flagellar motility (Miller et al., 2015). This is illustrated by striking differences in progesterone-elicited $I_{CatSper}$ responses in mouse and human (Lishko et al., 2011). Here we have shown that CatSper ε and ζ are components of the highly organized CatSper complex, that CatSperζ is required for proper continuity of this complex along the flagellum, and that loss of ζ alters hyperactivation waveforms and reduces fertilizing capacity.

The conservation pattern of the lineage-specific gain and loss of the ε gene is identical to those of β and γ, suggesting that they likely belonged to an ancient CatSper channel Ca^{2+} signaling network before the divergence of unikonts and bikonts. Since their protein expression is strictly interdependent, we speculate that ε-null mice will have the phenotype of *CatSper1-4*, or δ-null mice. In contrast, *CatSper*ζ is conserved only in mammals, suggesting that this protein imparts some adaptation, perhaps as a method enabling rheotaxis in the mammalian female reproductive tract.

Interestingly, although CatSperζ has no putative transmembrane domains, it is localized in the same quadrilateral pattern as other CatSpers, but is not present elsewhere in sperm. An intriguing aspect of our observations is that, unlike *CatSper1-4* and *δ*-null mice, which produce complete infertility, *CatSperζ*-null males exhibit an incomplete loss of fertility. The CatSper current is reduced in *CatSperζ*-null spermatozoa, and may have similar permeation properties (likely dominated by the CatSper1-4 pore subunits), but the effects of *CatSperζ* on channel gating remain to be determined in future studies. This is reminiscent of the non-spermatozoan, voltage-gated Ca_v channel auxiliary subunits, which are not required for expression but modulate expression levels and gating (Catterall et al., 2005). Most tantalizing is the thinning and disruption of the linear CatSper signaling domains at repeat intervals in the absence of ζ. Further detailed examination via mutagenesis experiments has been stymied by our inability to heterologously express functional CatSper channels. New rapid genome editing techniques should enable more mice to be generated that will further the study of CatSper trafficking, subunit interactions, and localized signaling pathways.

Traffic into the Linear Domains of Sperm Flagella

Functional Ca^{2+} signaling domains are common adaptations in many biological systems, such as synapses and muscle. They enable specific and fast triggering of downstream events (Clapham, 2007). CatSper channels are compartmentalized into a unique multilinear arrangement and form Ca^{2+} signaling nanodomains with other Ca^{2+} signaling molecules along the sperm flagellum (Chung et al., 2014). The mechanisms involved in delivery of the CatSper channels to these specific domains is currently unknown, and we suspect will be as interesting and complex as those in primary and motile cilia (Sung and Leroux, 2013). We found that abrogation of *CatSperζ* not only retards targeting of the CatSper complex to flagella, but also disrupts continuity of the linear domains, resulting in repeated fragmented domains with ~ 800 nm periodicity. In order for CatSper domains to form and function properly, interactions are needed between the CatSper channel complex in the flagellar membrane and the underlying cytoskeletal proteins. One speculation is that CatSperζ might adapt to cytoskeletal structures that traffic, distribute, and enable membrane insertion of CatSper.

The fibrous sheath (FS), a cytoskeletal structure unique to the mammalian sperm flagellum, defines the extent of the tail's principal piece, in which all the CatSper proteins are specifically localized. The FS closely lies under the plasma membrane and its two longitudinal columns are connected by circumferential ribs. Immunogold electron microscopy demonstrated that the CatSper channels are distributed on the end of ribs, where they merge with the column (Chung et al., 2014). It seems likely that timing of occurrence and localization of CatSper Ca^{2+} signaling domains is coordinated with the assembly of FS proteins along the axoneme. The column appears early in spermiogenesis, forming from the distal tip of the tail along the axoneme, followed by subsequent rib formation in the opposite direction (Oko, 1998; Oko and Clermont, 1989). Based on scanning electron micrographs (Danshina et al., 2010; Miki et al., 2004), we find that the distance between ribs is about 800 nm in mouse spermatozoa. Thus, it seems likely that the repeated disruption in the absence of *CatSperζ* is related to rib spacing of the FS.

Ca^{2+} Regulation of the Flagellar Envelope in Sperm Rheotaxis and Egg Penetration.

Genetic abrogation of CatSper disrupts hyperactivated motility as manifested by changes in movement symmetry, amplitude, and rolling (Carlson et al., 2003; Chung et al., 2011; Miki and Clapham, 2013; Qi et al., 2007). Here we report that the flagellar envelope is significantly altered in the absence of *CatSperζ*, in part due to the inflexibility of the proximal tail. We previously reported that the catalytic subunit of calcineurin, PP2B-Aγ, expresses throughout the tail but localized to the CatSper quadrilateral structures and axoneme (Chung et al., 2014). In *CatSper1*-null spermatozoa, PP2B-Aγ remains localized

primarily to the axoneme but disappears from the quadrilateral structures. Recently, a similar but not identical phenotype (inflexible midpiece, reduced hyperactivated motility, and impaired ZP penetration) was reported in testis-specific calcineurin *Ppp3cc*-null and *Ppp3r2*-null spermatozoa (Miyata et al., 2015) Note that the principal piece of both *CatSper1*-null and *Ppp3cc*-null spermatozoa are not rigid. The integrity and distribution of CatSper channels in *Ppp3cc*-null spermatozoa remain to be examined and may clarify midpiece/principal piece disparities. In any case, inflexibility in the proximal regions of flagellum results in a flagellar envelope approximated as a rod with a distal propeller. The sperm can rotate faster but the smaller lateral deviation reduces torque. This limits the sperm's ability to orient into the flow, as well as penetrate the cumulus and ZP.

Physiological Modulation of CatSper in Sperm Function and Fertility.

Gene-manipulated mice highlight the importance of *in vivo* observations and have reshaped the landscape of fertilization science (Okabe, 2015). *In vitro* capacitation and fertilization systems underpin much of the study of sperm motility and fertilization potential. While ejaculated sperm are preferred for fertilization studies in larger animals and humans, epididymal sperm are commonly used in genetically tractable mouse studies. Notably, these sperm are not exposed to accessory sex gland secretions and female fluids. This may explain why *CatSperζ*-null spermatozoa are completely infertile in an IVF setting (COCs), but *in vivo* are merely subfertile. Perhaps natural modulators, absent in epididymal sperm IVF studies, partially rescue the fertilizing potential of *CatSperζ*-null spermatozoa by activating Ca^{2+} signaling activity.

Interestingly, a transient pulse of Ca^{2+} can greatly reduce the capacitation time required for wt sperm to develop hyperactivated motility (Tateno, 2013). Moreover, Navarrete et al recently demonstrated that a short exposure to A23187 rescued the defects in motility and fertilizing capability of *CatSper1*-null sperm *in vitro* (Navarrete et al., 2016). These independent studies were interpreted to mean that the initial priming by Ca^{2+} influx, perhaps above a certain threshold, is essential for sperm function. However, the linear quadrilateral CatSper complexes are not present in *CatSper1*-null spermatozoa and in *CatSperζ*-null spermatozoa are disrupted by gaps. We hypothesize that the linear quadrilateral structure *in vivo* likely maintains, regulates, and distributes CatSper Ca^{2+} signaling during hyperactivated motility. But it is important to point out that alterations in the structure should also result in changes in mechanical properties, movement of the flagellum, distribution of entering calcium, and downstream kinase activity and the motor elements they regulate. This complexity is illustrated *in vivo* sperm swimming trajectories, which are modulated by switching between pro- and anti-hook beating patterns. In the absence of CatSper*ζ*, anti-hook beating predominates. Pro-hook motions are associated with intact CatSper-mediated Ca^{2+} signaling pathways (Chang and Suarez, 2011). Finally, ejaculated sperm display more pro-hook hyperactivation than epididymal sperm (Li et al., 2015).

Future areas for investigation are the functional positioning of the remaining accessory subunits of the CatSper channel in assembly and domain organization, the testing of potential modifiers present in accessory sex gland secretions that may activate CatSper channels, and the determination of Ca^{2+} dependent molecules in the axoneme which eventually determine flagellar bending and its envelope. *CatSperζ*-null mice, which are hypomorphic to the null-mutation of other CatSper genes with abrogated hyperactivation, and newly expanding animal models from recent advances in genome editing will serve as a foundation to this end. Advanced imaging techniques with higher time and spatial resolution will be necessary to carry this out. The present results also suggest that alterations of Ca^{2+} current and/or dysregulated downstream Ca^{2+} signaling affecting dynamic structures may be sufficient to compromise sperm function. CatSper's unique composition and central role in hyperactivated motility make it an ideal target for contraception.

Materials and Methods

Details of source and identifier are provided in the Key Resources Table as a supplementary file.

Animals

CatSper1 and *δ-null* mice were previously described (Chung et al., 2011; Ren et al., 2001). Lines were backcrossed and maintained on a C57BL/6 background. WT C57BL/6 male, B6D2F1 female (Jackson laboratory), and CD1 (Charles River) female mice were purchased.

Generation of CatSperζ-deficient mice and genotyping of mutant mice.

[1700019N12Rik$^{tm(KOMP)Mbp}$]-targeted ES cells (2 clones, 1700019N12Rik_D05 and 1700019N12Rik_C06) were purchased from the UC Davis KOMP repository. The parental ES cell line, JM8A1.N3, was derived from C57BL/6N (agouti) ES cells. Chimeras were born from injection of the C06 ES cells into host embryos. The male chimeras were bred to C57BL/6N females to establish germline transmission and obtain heterozygous animals. Initially, genotype analysis was performed by PCR on isolated genomic DNA (F/R1/R2, F (JJC575): 5'-ATAACCATCCGGGAGGAGAC-3', R1 (YS_zWT-Rev): 5'-GCGATGGTTTGCGTGTTTG-3', R2 (JJC562): 5'- CACAACGGGTTCTTCTGTTAGTCC-3'). From F2 mice, genotyping was done by Transnetyx. Mice used in this study were the offspring of crosses between F1 and/or F2 generations (100% C57BL/6N genetic background). Mice were treated in accordance with guidelines approved by the Boston Children's Hospital and Yale Animal Care and Use Committees (IACUC).

Mouse Sperm Preparation and *In Vitro* Capacitation

Mouse caudal epididymal sperm were collected by swim-out in HEPES buffered saline (HS) containing (in mM): 135 NaCl, 5 KCl, 2 $CaCl_2$, 1 $MgSO_4$, 20 HEPES, 5 glucose, 10 lactic acid, 1 Na pyruvate, pH 7.4 (with NaOH) (Chung et al., 2011). To induce capacitation *in vitro*, sperm cells were incubated (2 x 10^6 cells ml^{-1}) in human tubular fluid (HTF) media (in mM): 102 NaCl, 4.7 KCl, 2 $CaCl_2$, 0.2 $MgCl_2$, 0.37 KH_2PO_4, 2.78 glucose, 18.3 lactic acid, 0.33 Na pyruvate, 25 HCO_3^- and 4 mg ml^{-1} BSA) (Millipore) for 90 min at 37°C (5% CO_2).

Capacitation in varying external [Ca^{2+}].

To test the effect of external [Ca^{2+}] on the development of hyperactivated motility, 2 mM $CaCl_2$ in standard HTF was replaced with 4 mM, 0.5 mM, and 0.1 mM $CaCl_2$ and sperm cells were incubated for 90 min under capacitating conditions (37°C, 5% CO_2).

Motility rescue by Ca^{2+} ionophore, A23187 treatment. Ca^{2+} transient-inducible hyperactivated motility was tested by treating sperm with A23187 as described (Navarrete et al., 2016; Tateno et al., 2013) with slight modification. In short, caudal epididymal mouse sperm were collected by swim-out in HEPES-HTF medium (H-HTF: 92 mM NaCl, 2 mM $CaCl_2$, 4.7 mM KCl, 0.2 mM $MgCl_2$, 0.37 mM KH_2PO_4, 25 mM $NaHCO_3$, 18.3 mM Na lactate, 2.78 mM glucose, 0.33 mM Na pyruvate, 0.4% [w/v] bovine serum albumin [BSA], and 10 mM HEPES [pH 7.4]), allowing motile sperm to disperse for 10 min at 37 °C. Sperm concentration was ~ 4x10^7 cells/mL. An aliquot (150 µL) of the sperm suspension was exposed to 20 µM A23187 in H-HTF. After 10 min, sperm were washed by two centrifugation at 550 G for 5 min and 300 G for 5 min, resuspended in standard HTF, and incubated at 2x10^6 cells/ml under capacitating conditions (37 °C, 5% CO_2). At 5 min and 30 min post-incubation, spermatozoa were tethered to fibronectin-coated coverslips and recorded in H-HTF at 37°C as described in *Flagellar Waveform Analysis*.

Human Sperm Preparation

All experiments using human samples were approved by the Committee of Clinical Investigation, Boston Children's Hospital CCI/IRB (IRB-P00000538). Human semen samples were obtained from fertile donors.

Human spermatozoa were collected by the swim-up method with the use of modified human tubal fluid medium (HTF).

Cell line origin and authentication

HEK293T cells were purchased from ATCC. In this study, they were used to overexpress recombinant human CatSperζ in order to test antibodies. The cells were tested negative for mycoplasma and validated as of human origin. The identity was authenticated by confirming their negative expression of testis-specific genes including CatSper. The cell line was cultured in DMEM/F12 containing 10% FBS.

Antibodies and Reagents

Rabbit polyclonal CatSper1, CatSper4, β, and δ antibodies were previously described (Chung et al., 2011; Ren et al., 2001). To produce antibodies to new CatSper subunits, peptides were synthesized and conjugated to KLH carrier protein (Open Biosystems) as follows: mouse CatSperε, 968–985 (αm-ε968: RQFIIEPLHKRPAKQKKN); mouse CatSperζ, 174−195 (αm-ε174: GYIEGIRKRRNKRLYFLDQ); human CatSperε, 31−50 (αh-ε31: RIFSTRSTIKLEYEGTLFTE); and human CatSperζ, 11–29 (αh-ζ11: KSSDRQGSDEESVHSDTRD). Antisera were affinity purified on the immobilized resin of the corresponding peptide (Amino Link Plus or Sulfo Link Plus, Pierce). Anti-phosphotyrosine (clone 4G10), anti-Flag (clone M2), anti-calmodulin (05-173) and anti-acetylated tubulin (T7451) antibodies were from Sigma-Millipore. All chemical compounds were from Sigma-Aldrich unless indicated.

Genomic Database Search

Annotated orthologs in the NCBI gene database (http://www.ncbi.nlm.nih.gov/gene/) and/or homologous amino acid sequences of reported protein databases were screened in 17 eukaryotes for the presence of genes for CatSper auxiliary subunits. Non-annotated orthologs in the NCBI gene database were identified by comparing sequences of the annotated orthologs to those in the protein database of species by Phmmer implemented on HMMER 3.1 (default option, http://hmmer.org/). The longest amino acid sequences among all the isoforms of the orthologs annotated in each species and protein sequence databases from 15 eukaryotes, except human and mouse, were downloaded from the NCBI Genome database (http://www.ncbi.nlm.nih.gov/genome; *Tinamus guttatus,* GCA000705375.2; *Anolis carolinensis,* GCA000090745.2; *Salmo salar*, GCA000233375.4; *Callorhinchus milii*, GCA000165045.2; *Branchiostoma floridae*, GCA000003815.1; *Caenorhabditis elegans*, GCA000002985.3; *Crassostrea gigas*, GCA000297895.1; *Exaiptasia pallida*, GCA001417965.1; *Trichoplax adhaerens*; GCA000150275.1, *Salpingoeca rosetta*, GCA_000188695.1), Ensembl genome browser (http://ensembl.org; *Strongylocentrotus purpuratus*, GCA000002235.2; *Drosophila melanogaster*, GCA000001215.4; *Thecamonas trahens,* GCA000142905.1), and JGI genome portal (http://genome.jgi.doe.gov; *Allomyces macrogynus*; *Aurantiochytrium limacinum*). Aligned phmmer hits of expected values < 10^{-10} were considered as candidate orthologs of the corresponding CatSper subunits in each species.

Multiple tissue RT–PCR

PCR was performed according to standard protocols using a commercial multiple panel cDNA template (MTC, Clontech). PCR primers amplified *Gm7068* (forward: 5′-CTATGGCTCAAGTGTAATGACC-3′, reverse: 5′-GCTCTTATTGAATCCTCGAACC-3′), *Tex40* (forward: 5′-GAAACAGGATTCGCAAGTACAG-3′, reverse: 5′-TCGTGGACCTATATGTGATGAG-3′) using mouse *GAPDH* (forward: 5′-TGAAGGTCGGTGTGAACGGAT-TTGGC-3′, 5′-ATGTAGGCCAT GAGGTCCACCAC-3′) as a control.

Molecular cloning

The initial mouse *Tex40* cDNA sequence (NM_001039494) was identified from database searches using novel peptide sequences from MS. Full-length human *Tex40* cDNAs was obtained by PCR with primers

(forward: 5′-GGGCAGAACCATGGAGGAAA-3′, reverse: 5′-AGGACTCAAATTCCACTCGGATG-3′) using the human testis cDNA library (Clontech). Sequencing the TOPO-cloned PCR products into pCR4-TA (Invitrogen) confirmed the full-length human *Tex40* ORF, which was subcloned into pCMV-Tag2A (Stratagene) to express recombinant N-terminal Flag-tagged human CatSperζ in mammalian cells. Mouse *Gm7068* was identified by homologous amino acid sequence to C-terminal *CatSperδ* (Tmem146). There are six transcript variants (1; XM_006497083, 2; XM_006497084, 3; XM_017314031, 5: XM_006497085, 6; XM_017314033, and 8; XM_006497087). Variants 1, 3, 5, 6, and 8 are predicted to encode polypeptides with the same very C-terminal sequence that can be detected by anti-mε-968. Among them, the predicted polypeptides from longer splicing variant 1 (isoform X1; XP_006497147, 985 aa) and variant 3 (isoform X3; XP_017169520, 914 aa) are consistent with the apparent molecular weight of the band observed in testes microsomes (Figures 4B and S2D). The predicted polypeptides from shorter variant 5 (isoform 4; XP_006497148, 805 aa) and variant 6 (isoform 5; XP_017169522, 770 aa) are consistent with that of the band detected in CatSper1-IP from testis and total sperm lysate (Figures 1D, 1E and 4A). It is likely that mouse Gm7068 expresses at least 4 potential splice variants that can encode proteins isoforms and/or undergo cleavage during spermatogenesis.

RNA *In situ* hybridization

In situ hybridization experiments were carried out with an RNAscope (Advanced Cell Diagnostics). Testes from 3 month old wild-type mice were fixed in 10% (vol/vol) neutral-buffered formalin at room temperature for 24 h, dehydrated, and embedded in paraffin. Paraffin sections (10-μm thick) were processed according to the manufacturer's instructions for *in situ* detection in the Rodent Histopathology Core Facility at Harvard Medical School. Sequences of the probes used in this study are: Gm7068 (XM_982472.3, 645 – 1072) and Tex40 (NM_001039494.2, 41- 456). After the DAB (3,3, -diaminobenzidine) reaction, slides were counterstained using hematoxylin.

mRNA Preparation & Real-Time PCR

Real-time PCR was carried out with first strand cDNAs (iScript cDNA Synthesis, Bio-Rad) synthesized from 2 μg total mouse testis RNA using the SYBR Green (iTaq Universal SYBR Green Supermix, Bio-Rad; CFX96). Quantitative analysis by the dd*Ct* method employed c-Jun as an amplification control. Three independent sets of experiments were performed to calculate fold changes (2^{-ddCt}) of *CatSpers* mRNA. The primers used for qRT-PCR were: *CatSper1* (forward: 5′-CTGCCTCTTCCTCTTCTCTG-3′, reverse: 5′-TGTCTATGTAGATGAGGGACCA-3′), *CatSperβ* (forward: 5′-CCTTA TTGACCAAGAAACAGAC-3′, reverse: 5′-TGAAACCCATATTTGACTGCC-3′), *CatSperγ* (forward: 5′-TGAGCAATAGAGGTGTAGAC-3′, reverse: 5′-CAGGA TGTAGAAGACAACCAG-3′), *CatSperδ* (forward: 5′- GCTGACATTTCTGTGTATCTAGG-3′, reverse: 5′-CTGATATACCTTCCAATTTACGCC-3′), *CatSperε* (forward: 5′- GTCTCATGCTTCTTCAGTTCC-3′, reverse: 5′-CAGAAGTTCCTTGTCCATCAC-3′), *CatSperζ* (forward: 5′-GAGACCTCCTTAGCATCGTC-3′, reverse: 5′-TCGTGGACCTATATGTGATGAG-3′ and *c-Jun* (forward: 5′- CTC CAG ACG GCA GTG CTT -3′, reverse: 5′- GAG TGC TAG CGG AGT CTT AAC C -3′).

Preparation of Mouse Testis Microsome

Testes (200 mg, normally two testicles) from 8- to 12-wk-old male mice were homogenized on ice using a Dounce homogenizer in 2 mL 0.32 M sucrose solution with protease inhibitor cocktails (Roche). The tissue suspension was centrifuged at 300 g for 10 min at 4°C and the supernatant was then transferred to an ultra-speed centrifuge tube. The microsome faction was isolated by centrifuging the tube at 105,000 g for 60 min.

Protein Preparation, Immunoprecipitation, and Western Blotting. Mouse sperm total protein was prepared as described before (Chung et al., 2011; Chung et al., 2014). For total protein from human spermatozoa, purified swim-up sperm were then lysed (0.1% SDS, 0.5% sodium deoxycholate, 1 mM

DTT, 1 mM EDTA in PBS with protease inhibitors) followed by sonication for 5 min and centrifuged at 15,000 g for 10 min. The supernatants were further denatured by adding DTT to 10 mM and heated at 75^{o}C for 10 min before SDS-PAGE. For immunoprecipitation, the testis microsome pellet was resuspended in 10 mL 1% Triton X-100 in PBS with protease inhibitors (Roche). The suspension was rocked at 4°C for 1 h and then centrifuged at 15,000 g for 30 min. 1.5 mL of the solubilized testis microsome were mixed with 1-2 µg antibody and 25 µL Protein A/G-bead slurry (Santa Cruz Biotechnology) at 4°C overnight. The IP products were finally eluted in 50 µL LDS loading buffer containing 50 mM DTT. Antibodies used for Western blotting were rabbit anti-mouse CatSperε (αm-ε968; 1.6 µg/mL), mouse CatSperζ (αm-ε174; 2.7 µg/mL), human CatSperε (αh-ε31; 2.7 µg/mL), human CatSperζ (αh-ζ11: 1 µg/mL). Monoclonal anti-phosphotyrosine (clone 4G10; 1 µg/mL), anti-Flag (clone M2; 1 µg/mL), anti-calmodulin (05-173, 1 µg/mL), and anti-acetylated tubulin (T7451,1: 20,000). Secondary antibodies were anti-rabbit IgG-HRP (1:10,000) and anti-mouse IgG-HRP (1: 10,000) from Jackson ImmunoResearch.

Sperm Immunocytochemistry

Caudal epididymal mouse sperm cells attached to glass coverslips were fixed in 4% paraformaldehyde (PFA) in PBS, permeabilized with 0.1% TrixonX-100 for 10 min. Human sperm cells from swim-up purification were fixed 4% PFA in PBS for 10 min followed by 100% MeOH. Fixed human sperm cells were permeabilized in 0.1% saponin for 10 min. Permeabilized sperm cells were washed in PBS and blocked with 10% goat serum for 1 h. Mouse samples were stained overnight with primary antibody against CatSper1 (10 µg ml^{-1}) and CatSperζ (mζ174, 20 µg ml^{-1}) as were human samples with primary antibodies against CatSperε (hε31, 20 µg ml^{-1}) and CatSperζ (hζ11, 10 µg ml^{-1}), in 10% goat serum in PBS, 4°C. After PBS wash, goat-anti-rabbit Alexa488 conjugate (Invitrogen) served as the secondary antibody. Images were acquired on laser scanning confocal microscopes (Olympus Fluoview 1000; Figures 1G, 1H, S2G, and S3E and Leica TCS SP8; deconvolved image in Figure 5A).

Super-resolution Imaging

3D STED imaging

For analysis of CatSper nanodomain organization, CatSper1 images were acquired with Leica TCS SP8 gated stimulated emission and depletion (STED 3×) microscopy using an HCX PL APO 100×/1.40 oil objective lens (Leica Microsystems). Samples were prepared as described in *Sperm Immunocytochemistry* with slight modifications. After incubation with primary antibody, cells were washed with PBS and incubated with goat anti-rabbit IgG coupled to Alexa Fluor 546 (Invitrogen, 1:100) for 1 h at room temperature. Coverslips were mounted with Prolong Gold (Invitrogen) and cured for 24 h before image acquisition. Within each experiment, identical settings for laser power, STED power, and gating were used to acquire images. The wavelength of the STED depletion laser was 660 nm and was adjusted to 50% of power. z-stacks of 17 optical sections with a step size of 0.1 µm were deconvolved using Huygens Software.

3D STORM Imaging

3D STORM experiments were performed as previously described (Chung et al., 2014). Imaging buffer was prepared in 60% (wt/wt) sucrose solution, increasing imaging depth to 1 µm (Chung et al., 2014). Imaging buffer was supplemented with 100 mM mercaptoethylamine (pH 8.5) as a switching agent as well as an O_2 scavenger (5% glucose (wt/vol), 0.5 mg/ml glucose oxidase, and 40 mg/ml catalase) to reduce the rate of photobleaching. The sample was illuminated at 657 nm for imaging the photoswitchable reporter molecules (Alexa 647), and 405 or 532 nm for facilitating the activation of Alexa 647 from the dark state. For 3D localization, a cylindrical lens (focal length = 1 m) was inserted into the detection path to enable determination of *z* positions from the ellipticities of the molecular images and the *x* and *y* positions from the centroid positions (Huang et al., 2008). Image analysis and rendering was performed and angular profiles were constructed as previously described (Chung et al., 2014).

Fourier Transform and Autocorrelation

Fourier transform and autocorrelation analyses of 3D STORM images were performed as previously described (Xu et al., 2013; Zhong et al., 2014). A Fourier transform of the 1D projection localization distribution yielded a main peak that corresponds to a spatial period of ~800 nm for the CatSperζ-/- spermatozoa. The autocorrelation curve for the CatSperζ-/- spermatozoa showed a periodic modulation with the first peak at ~850 nm.

Sperm Migration Assay & In Vivo Fertilization

For timed coitus, females were introduced to single-caged *CatSperζ-Het* or *-null* males for 1 h and checked for the presence of a vaginal plug. To examine sperm migration to the fertilization site *in vivo,* ampullae were removed from the mated females at 8 h after coitus and COCs were released. A series of *z*-stacked images (2-μm step size) of the COCs was taken and number of sperm within each COC was recorded according to the presence of a sperm head. To calculate *in vivo* fertilization rate, eggs were gently flushed from oviducts and ampullae from the mated females at 20 h and 27-30 h after coitus. The total number of eggs and the number of 2-cell eggs were counted.

Fertility test and *in vitro* fertilization

Two females were caged with each male for 3 months to track pregnancy and litter production. For IVF assays, oocytes were recovered from superovulated 5-6-week-old B6D2F1 female mice 13 h after injection of 5 U human chorionic gonadotropin. For standard IVF, sperm were collected from the *cauda epididymis*. For ejaculate IVF, sperm were retrieved from the uterus of a 1 h window-timed coitus. Both epididymal and ejaculated sperm were capacitated *in vitro* at 37°C for 1 h, and coincubated with eggs at ~10^5 sperm/mL. After about 4.5 h, unbound sperm were washed away. After 24 h incubation the embryos were observed under light microscopy (Olympus IX-70) to check for development of the two-cell stage.

Flagellar waveform analysis

Spermatozoa from dissected *cauda* epididymis (swim up method) were collected in HEPES buffered saline (HS) media. Spermatozoa were plated on 35 mm fibronectin-coated coverslips for 15 min (22°C); unattached sperm were removed by gentle pipette wash (time 0) and basal motility recorded. Activated motility was recorded within the first 10 min after adding pre-warmed human tubal fluid (HTF)-capacitating medium (Millipore). To induce hyperactivation, attached sperm cells were incubated in HTF media for 90 min at 37°C (5% CO_2). All subsequent images were recorded at 37°C. The flagellar waveform was analyzed by stop-motion digital imaging collected at 200 fps (HC Image software, Hamamatsu Photonics or Zen Blue, Zeiss; 2 s movies). Overlay of flagellar traces from two complete flagellar beats were generated by hyperstacking binary images using open-source FIJI software (Schindelin et al., 2012) and time coded in color.

Sperm motility analysis

Cauda epididymal spermatozoa were suspended and incubated in non-capacitating M2 medium (Specialty Media, Millipore) or in HTF medium for capacitation. Sperm motility was then measured using the IVOS sperm analysis system (Hamilton Thorne Biosciences, Beverly, MA) in an 80-μm (depth) chamber to obtain various parameters (**Figure S4D**). Sperm motility was also analyzed with an Olympus IX-70 microscope equipped with a high-speed sCMOS camera (Orca-Flash4.0) and a 10x objective. 1–2 x 10^5 mouse sperm before and after capacitation were added to the 37°C chamber (Delta T culture dish controller; Bioptechs) containing 1 ml HEPES-HTF medium (H-HTF: 92 mM NaCl, 2 mM $CaCl_2$, 4.7 mM KCl, 0.2 mM $MgCl_2$, 0.37 mM KH_2PO_4, 25 mM $NaHCO_3$, 18.3 mM Na lactate, 2.78 mM glucose, 0.33 mM Na pyruvate, 0.4% [w/v] bovine serum albumin [BSA], and 10 mM HEPES [pH 7.4]). In some experiments, the medium was supplemented with methylcellulose (MC) (M0512, 4,000 cP in 2% solution; Sigma) at

0.3%, 0.4%, or 0.5% (w/v). Sperm swimming 3–5 mm from the rim were recorded after a 10 min preincubation period that allowed spontaneous dissociation of sperm clumps. To inhibit convective flow, 1 ml of medium was overlaid by 1 ml of mineral oil and covered by a heated glass lid (Bioptechs). Sperm motility at 37°C was videotaped at 100 fps. Images (HC Image software, Hamamatsu Photonics) were analyzed for swimming trajectory from a 1 s playback movie at 1/5 speed, by head tracing via Computer Assisted Sperm Analysis (CASA; http://rsbweb.nih.gov/ij/plugins/casa.html). To track swimming trajectory in viscous medium, the sperm motility was videotaped at 50 fps. The images were analyzed using Fiji software (Schindelin et al., 2012) by assembling overlays of the flagellar traces generated by hyperstacking binary images of 20 frames of 2 s movies coded in a gray intensity scale.

In-Capillary Sperm Rheotaxis

Mouse sperm incubated in HTF medium for 90 min at 2x 10^6/ml yielded capacitated sperm. Capacitated sperm were transferred and concentrated for capillary loading by centrifugation at 900 g for 3 min. The loose sperm pellet at the bottom of the microcentrifuge tube was resuspended in HEPES-HTF at 4 x 10^6/ml, and loaded into the capillary by suction via an air-pressure microinjector (IM-5B; Narishige; 22 C, ~ 200 µm/s). While applying gentle positive pressure, the sperm in the tip of the capillary were moved out of the sperm drop. The tip of capillary is transferred to a 37°C chamber (Delta T culture dish controller; Bioptechs) and placed into a 50 µl drop of HEPES-HTF medium covered with mineral oil. Negative pressure was applied slowly and sperm cells swimming against the flow and down to the H-HTF drop was video-recorded at 33 fps.

Electrophysiological recording of mouse spermatozoa.

Whole-cell recording of *corpus epididymal* spermatozoa from 3-5 month-old *CatSperζ*+/- or *CatSperζ*-/- mice was performed blind as to genotype (Kirichok et al., 2006; Navarro et al., 2011). HS was the bath medium. The standard pipette solution was (mM): 120 Cs- Methanesulfonate (Cs-$MeSO_4$), 5 CsCl, 5 Cs-BAPTA, 10 HEPES and 10 MES, pH 7.2 with H-$MeSO_3$. To record I_{ATP}, we used a low Cl^- bath solution (to reduce background Cl^- conductance) in the following (mM): 150 Na- methanesulfonate (Na-$MeSO_3$), 2 $CaCl_2$, 10 Na-HEPES, and 10 MES (pH 7.4 or 6.0). To measure $I_{CatSper}$, we used divalent-free (DVF) solution, in mM: 150 Na-$MeSO_3$, 2 Na_3HEDTA [(hydroxyethyl)ethylenediaminetriacetic acid], 2 EGTA, and 20 HEPES (pH 7.4) with NaOH. Solutions were applied to sperm cells (lifted from the coverslips) initially by bath perfusion. After break-in, the access resistance was 25–80 MΩ. All experiments were performed at 22–24 °C. The whole-cell currents were recorded using an Axopatch 200B amplifier (Molecular Devices), acquired with Clampex 9 (pClamp9 Software; Molecular Devices), and analyzed with Origin software (OriginLab). Signals were low-pass filtered at 2 kHz and sampled at 10 kHz. Data are given as mean ± SD.

Quantification and Statistical Analysis

All the experiments are repeated at least 3 times. Sample size and number of replicates are described in each figure and the figure legends. Statistical analyses were performed using Student's t-test unless indicated; e.g. F-test in one-way ANOVA. Differences were considered significant at $*P < 0.05$, $**P < 0.01$, $***P < 0.001$, and $****P < 0.0001$. When $****P < 0.0001$, actual P value is not indicated.

Acknowledgments

We thank M. Sanguinetti for testing CatSper expression in *Xenopus* oocytes for $I_{CatSper}$ detection, P. DeCaen for help with sperm electrophysiology, and L. Ded for calculating rib length from the literature and critical reading of the manuscript-in-progress. This work was supported by Goodman-Gilman Yale Scholar Award 2015-08 (J.-J.C.), HHMI (X.Z.), and HHMI (D.E.C.).

Competing Interest

We declare that none of the authors have a financial interest related to this work.

Author Contributions

J.-J.C. conceived the project and designed experiments. J.-J.C, K.M., D.K., S.-H.S., and J.Y.H. performed and analyzed experiments. J.-J.C. did mouse genetics, gene expression studies, protein biochemistry including immunoblotting (H.F.S.), confocal imaging, STED imaging, *in vitro* and *in vivo* fertilization assays (Y.I. and H.F.S.), sperm motility and waveform analyses (J.Y.H.), rheotactic measurement of sperm (K.M. and H.F.S.) and contributed to all of the STORM imaging experiments. K.M. did electrophysiological recording. D.K. and S.-H.S. performed STORM imaging, image analysis, and rendering. J.Y.H. and X.C. did comparative genomic analysis. X.Z. advised D.K. and S.-H.S. on STORM experiments. J.-J.C. and D.E.C. supervised the project. J.-J.C. and H.F.S. assembled figures, and J.-J.C. and D.E.C. wrote the manuscript with the input from the co-authors.

References

Almers, W., McCleskey, E.W., and Palade, P.T. (1984). A non-selective cation conductance in frog muscle membrane blocked by micromolar external calcium ions. J Physiol *353*, 565-583.

Cai, X., and Clapham, D.E. (2008). Evolutionary genomics reveals lineage-specific gene loss and rapid evolution of a sperm-specific ion channel complex: CatSpers and CatSperbeta. PLoS One *3*, e3569.

Cai, X., Wang, X., and Clapham, D.E. (2014). Early evolution of the eukaryotic Ca2+ signaling machinery: conservation of the CatSper channel complex. Mol Biol Evol *31*, 2735-2740.

Carlson, A.E., Westenbroek, R.E., Quill, T., Ren, D., Clapham, D.E., Hille, B., Garbers, D.L., and Babcock, D.F. (2003). CatSper1 required for evoked Ca2+ entry and control of flagellar function in sperm. Proc Natl Acad Sci U S A *100*, 14864-14868.

Catterall, W.A., Perez-Reyes, E., Snutch, T.P., and Striessnig, J. (2005). International Union of Pharmacology. XLVIII. Nomenclature and structure-function relationships of voltage-gated calcium channels. Pharmacol Rev *57*, 411-425.

Chang, H., and Suarez, S.S. (2011). Two distinct Ca(2+) signaling pathways modulate sperm flagellar beating patterns in mice. Biol Reprod *85*, 296-305.

Chung, J.J., Navarro, B., Krapivinsky, G., Krapivinsky, L., and Clapham, D.E. (2011). A novel gene required for male fertility and functional CATSPER channel formation in spermatozoa. Nat Commun *2*, 153.

Chung, J.J., Shim, S.H., Everley, R.A., Gygi, S.P., Zhuang, X., and Clapham, D.E. (2014). Structurally distinct Ca(2+) signaling domains of sperm flagella orchestrate tyrosine phosphorylation and motility. Cell *157*, 808-822.

Clapham, D.E. (2007). Calcium signaling. Cell *131*, 1047-1058.

Danshina, P.V., Geyer, C.B., Dai, Q., Goulding, E.H., Willis, W.D., Kitto, G.B., McCarrey, J.R., Eddy, E.M., and O'Brien, D.A. (2010). Phosphoglycerate kinase 2 (PGK2) is essential for sperm function and male fertility in mice. Biol Reprod *82*, 136-145.

Demott, R.P., and Suarez, S.S. (1992). Hyperactivated sperm progress in the mouse oviduct. Biol Reprod *46*, 779-785.

Frank, K., and Sippl, M.J. (2008). High-performance signal peptide prediction based on sequence alignment techniques. Bioinformatics *24*, 2172-2176.

Ho, K., Wolff, C.A., and Suarez, S.S. (2009). CatSper-null mutant spermatozoa are unable to ascend beyond the oviductal reservoir. Reprod Fertil Dev *21*, 345-350.

Huang, B., Wang, W., Bates, M., and Zhuang, X. (2008). Three-dimensional super-resolution imaging by stochastic optical reconstruction microscopy. Science *319*, 810-813.
Ishijima, S. (2011). Dynamics of flagellar force generated by a hyperactivated spermatozoon. Reproduction *142*, 409-415.
Ishijima, S., Baba, S.A., Mohri, H., and Suarez, S.S. (2002). Quantitative analysis of flagellar movement in hyperactivated and acrosome-reacted golden hamster spermatozoa. Mol Reprod Dev *61*, 376-384.
Kirichok, Y., Navarro, B., and Clapham, D.E. (2006). Whole-cell patch-clamp measurements of spermatozoa reveal an alkaline-activated Ca2+ channel. Nature *439*, 737-740.
Li, H., Hung, P.H., and Suarez, S.S. (2015). Ejaculated mouse sperm enter cumulus-oocyte complexes more efficiently in vitro than epididymal sperm. PLoS One *10*, e0127753.
Lishko, P.V., Botchkina, I.L., and Kirichok, Y. (2011). Progesterone activates the principal Ca2+ channel of human sperm. Nature *471*, 387-391.
Liu, J., Xia, J., Cho, K.H., Clapham, D.E., and Ren, D. (2007). CatSperbeta, a novel transmembrane protein in the CatSper channel complex. J Biol Chem *282*, 18945-18952.
Miki, K., and Clapham, D.E. (2013). Rheotaxis guides mammalian sperm. Curr Biol *23*, 443-452.
Miki, K., Qu, W., Goulding, E.H., Willis, W.D., Bunch, D.O., Strader, L.F., Perreault, S.D., Eddy, E.M., and O'Brien, D.A. (2004). Glyceraldehyde 3-phosphate dehydrogenase-S, a sperm-specific glycolytic enzyme, is required for sperm motility and male fertility. Proc Natl Acad Sci U S A *101*, 16501-16506.
Miller, M.R., Mansell, S.A., Meyers, S.A., and Lishko, P.V. (2015). Flagellar ion channels of sperm: similarities and differences between species. Cell Calcium *58*, 105-113.
Miyata, H., Satouh, Y., Mashiko, D., Muto, M., Nozawa, K., Shiba, K., Fujihara, Y., Isotani, A., Inaba, K., and Ikawa, M. (2015). Sperm calcineurin inhibition prevents mouse fertility with implications for male contraceptive. Science *350*, 442-445.
Navarrete, F.A., Alvau, A., Lee, H.C., Levin, L.R., Buck, J., Leon, P.M., Santi, C.M., Krapf, D., Mager, J., Fissore, R.A*., et al.* (2016). Transient exposure to calcium ionophore enables in vitro fertilization in sterile mouse models. Sci Rep *6*, 33589.
Navarrete, F.A., Garcia-Vazquez, F.A., Alvau, A., Escoffier, J., Krapf, D., Sanchez-Cardenas, C., Salicioni, A.M., Darszon, A., and Visconti, P.E. (2015). Biphasic role of calcium in mouse sperm capacitation signaling pathways. J Cell Physiol *230*, 1758-1769.
Navarro, B., Kirichok, Y., and Clapham, D.E. (2007). KSper, a pH-sensitive K+ current that controls sperm membrane potential. Proc Natl Acad Sci U S A *104*, 7688-7692.
Navarro, B., Miki, K., and Clapham, D.E. (2011). ATP-activated P2X2 current in mouse spermatozoa. Proc Natl Acad Sci U S A *108*, 14342-14347.
Okabe, M. (2015). Mechanisms of fertilization elucidated by gene-manipulated animals. Asian J Androl *17*, 646-652.
Oko, R. (1998). Occurrence and formation of cytoskeletal proteins in mammalian spermatozoa. Andrologia *30*, 193-206.
Oko, R., and Clermont, Y. (1989). Light microscopic immunocytochemical study of fibrous sheath and outer dense fiber formation in the rat spermatid. Anat Rec *225*, 46-55.
Qi, H., Moran, M.M., Navarro, B., Chong, J.A., Krapivinsky, G., Krapivinsky, L., Kirichok, Y., Ramsey, I.S., Quill, T.A., and Clapham, D.E. (2007). All four CatSper ion channel proteins are required for male fertility and sperm cell hyperactivated motility. Proc Natl Acad Sci U S A *104*, 1219-1223.

Quill, T.A., Sugden, S.A., Rossi, K.L., Doolittle, L.K., Hammer, R.E., and Garbers, D.L. (2003). Hyperactivated sperm motility driven by CatSper2 is required for fertilization. Proc Natl Acad Sci U S A *100*, 14869-14874.

Ren, D., Navarro, B., Perez, G., Jackson, A.C., Hsu, S., Shi, Q., Tilly, J.L., and Clapham, D.E. (2001). A sperm ion channel required for sperm motility and male fertility. Nature *413*, 603-609.

Schindelin, J., Arganda-Carreras, I., Frise, E., Kaynig, V., Longair, M., Pietzsch, T., Preibisch, S., Rueden, C., Saalfeld, S., Schmid, B*., et al.* (2012). Fiji: an open-source platform for biological-image analysis. Nat Methods *9*, 676-682.

Smith, J.F., Syritsyna, O., Fellous, M., Serres, C., Mannowetz, N., Kirichok, Y., and Lishko, P.V. (2013). Disruption of the principal, progesterone-activated sperm Ca2+ channel in a CatSper2-deficient infertile patient. Proc Natl Acad Sci U S A *110*, 6823-6828.

Stauss, C.R., Votta, T.J., and Suarez, S.S. (1995). Sperm motility hyperactivation facilitates penetration of the hamster zona pellucida. Biol Reprod *53*, 1280-1285.

Sung, C.H., and Leroux, M.R. (2013). The roles of evolutionarily conserved functional modules in cilia-related trafficking. Nat Cell Biol *15*, 1387-1397.

Swanson, W.J., and Vacquier, V.D. (2002). The rapid evolution of reproductive proteins. Nat Rev Genet *3*, 137-144.

Tateno, H., Krapf, D., Hino, T., Sanchez-Cardenas, C., Darszon, A., Yanagimachi, R., and Visconti, P.E. (2013). Ca2+ ionophore A23187 can make mouse spermatozoa capable of fertilizing in vitro without activation of cAMP-dependent phosphorylation pathways. Proc Natl Acad Sci U S A *110*, 18543-18548.

Torgerson, D.G., Kulathinal, R.J., and Singh, R.S. (2002). Mammalian sperm proteins are rapidly evolving: evidence of positive selection in functionally diverse genes. Mol Biol Evol *19*, 1973-1980.

Xu, K., Zhong, G., and Zhuang, X. (2013). Actin, spectrin, and associated proteins form a periodic cytoskeletal structure in axons. Science *339*, 452-456.

Yanagimachi, R. (1966). Time and process of sperm penetration into hamster ova in vivo and in vitro. J Reprod Fertil *11*, 359-370.

Zhong, G., He, J., Zhou, R., Lorenzo, D., Babcock, H.P., Bennett, V., and Zhuang, X. (2014). Developmental mechanism of the periodic membrane skeleton in axons. Elife *3*.

Figure legends

Figure 1. CatSper ε and ζ, Two New Accessory Proteins of CatSper Channel Complex. (A and B) Mouse protein sequences of CatSper ε (A) and CatSper ζ (B). (C) Cartoon of the predicted topology of 9 CatSper subunits. (D) Association of CatSper ε with CatSper1 in testis. (E and F) Dependence of CatSper ε (E) and ζ (F) proteins on CatSper1 in mouse sperm cells. (G and H) Confocal fluorescence and the corresponding phase-contrast images of immunostained human CatSper ε (G) and mouse CatSper ζ (H). (I) 3D STORM images of mouse CatSperζ in capacitated wt sperm. *x-y* projection (left) and a *y-z* cross-section (right) at 0.5 um from the annulus. The color encodes the relative distance from the focal plane along the *z* axis (color scale bar in *x-y* projection). (J) 3D STORM images of human CatSper ε in *x-y* projection (left), in *y-z* cross-sections (right). Colors indicate the *z* positions (see color scale bar). See also **Figure 1-figure supplements 1-2**.

Figure 1-figure supplement 1. Identification of CatSper ε and ζ, Two Novel Accessory Proteins of the CatSper Channel Complex, Related to Figure 1. (A) Multiple sequence alignment of CatSper δ identifies C1orf101 as δ homologs from various species. Alignments originate ~165 amino acids before the predicted single transmembrane (TM) domain, showing the highly conserved region in the proteins' C-terminal half. Identical (black) and similar (gray) residues highlighted. (B) CatSper ε is a protein containing a putative single transmembrane (TM) domain localized to the sperm tail. Pairwise alignment of the predicted human (upper, C1orf101 isoform 1) and mouse (lower, C1orf101-like isoform X2) CatSper ε protein sequences. The predicted signal peptide (SP) (Frank and Sippl, 2008) and TM domain are boxed. (C) von Heijne hydrophilicity plot (window size =11) of human and mouse CatSper ε proteins. (D) Sequence alignment between the human (upper) and mouse (lower) CatSper ζ proteins encoded by *Tex40* genes. The 4 peptides from mouse CatSper ζ (identified by mass spectrophotometry from CatSper1 affinity purification but not annotated in the previous study) (Chung et al., 2011), are underlined.

Figure 1-figure supplement 2. Expression of *CatSper ε* and *ζ* mRNAs and proteins, Related to Figure 1. (A) Tissue expression profile of *CatSper ε* and *ζ*. Reverse transcription PCR of *CatSper ε* (upper), *ζ* (middle), and *G3pdh* (control; lower) from 12 mouse cDNAs. *CatSper ε* and *ζ* are enriched in testis. (B) Spatial localization of *CatSperε* and *ζ* mRNA in the testis. Representative fields of *in situ* hybridization by gene-specific oligonucleotides against *CatSperε* (left) and *ζ* (right) in mouse testis (RNAscope). (C) Temporal expression of *CatSper1*, *CatSperε*, and *CatSperζ* mRNAs during postnatal testis development. The mRNA levels of *CatSper1* (orange), *CatSperε* (green), and *CatSperζ* (blue) are measured by real-time RT PCR, normalized to HPRT and expressed as ratios relative to 80-day old adult mouse testis. The data are presented as mean ± SEM. N=3. (D) Partitioning of CatSperε and CatSperζ in fractionated extracts of testis from wt mice. Both CatSperε and CatSperζ are enriched in the microsomal pellet (P), not in supernatant (S). (E-G) Specific recognition of CatSperε and CatSperζ in human spermatozoa. Immunoblotting of (E) total human sperm extracts and (F) recombinant human CatSperζ by rabbit polyclonal CatSperε (hε31) and CatSperζ (hζ11) antibodies, respectively. d1 and d2 indicate sperm from donors 1 and 2. (G) Confocal image and the corresponding phase-contrast image of CatSperζ in human sperm, immunostained with hζ11.

Figure 2. Deletion of the Mouse CatSperζ Subunit Severely Impairs Male Fertility. (A) Percent pregnancy rate over 3 months. (B) Average litter size resulting from *CatSperζ*+/- (7.4 ± 0.5) and *CatSperζ*-/- (4.4 ± 0.3) males. (C) Sperm number per egg at the fertilization site 8 h after 1 h window-timed coitus with *CatSperζ*+/- (0.58 ± 0.15) and *CatSperζ*-/- (0, none) males, quantified from eggs collected from ampullae. (B) and (C) Data are mean ± SEM. ****$P < 0.0001$. (D) *In vivo* fertilization rate:

Scatter plot with mean % of 2-cell fertilized eggs from *CatSperζ*+/- (70% and 94.4%) and *CatSperζ*-/- (21.3% and 24.6%) mated females at 20 and 27-30 h after coitus, respectively. (E) Head trace of free swimming *CatSperζ*+/- (top) and *CatSperζ*-/- (bottom) sperm cells at 10 min (left) and 90 min (right) after capacitation. Traces are from 1 s movies taken at 37°C. (F) Flagellar waveform traces. Movies recorded at 200 fps: *CatSperζ*+/- (top) and *CatSperζ*-/- (bottom) sperm cells attached on glass coverslips before capacitation (left), and 10 min (middle), and 90 min (right) after capacitation. Overlays of flagellar traces from two beat cycles are generated by hyperstacking binary images; time coded in color. See also **Figure 2-figure supplements 1-2** and **Figure 6-figure supplement 1**.

Figure 2-figure supplement 1. Generation of *CatSperζ*-/- mice, Related to Figure 2. (A) Distribution of CatSper subunits in eukaryotes. (B) ES cells (Project ID: CSD33943) from the KOMP Repository were used to produce KO mice. Exons 2-4 deleted by gene trap. (C and D) Genotyping (primers F/R1/R2) (C) and immunoblotting (D) analysis of *CatSperζ*-/-. (E) Normal sperm morphology despite the absence of ζ protein in *CatSperζ*-/- spermatozoa. Overlay of confocal images and the corresponding phase-contrast images of mouse sperm cells from *CatSperζ*+/- and *CatSperζ*-/- mice immunostained with mζ174 (also used in (D) and **Figure 1F** and **1H**. Principal piece labeling is not observed in *CatSperζ-null* sperm, validating the specific subcellular distribution of the signal to the sperm tail. Hoechst dye stains the sperm head DNA (blue).

Figure 2-figure supplement 2. Sperm Count and Fertility of *CatSperζ*-/- Mice; Sperm Motility Analysis and Development of P-Tyr, Related to Figures 2 and 3. (A) Epididymal sperm count (mean ± SEM) from littermates at ages 2-3 months. *CatSperζ* het *(+/-,* blue; 2.4 ± 0.1) versus null *(-/-,* green; 2.4± 0.2) cells (10^7). (B) Average litter size from all males in the mating test, grouped by male and female genotype. (C) IVF rate calculated by counting fertilized eggs (2-cell stage) 20 and 27-30 h after coitus. Data are expressed as scatter plot of mean percentage from *CatSperζ*+/- (20h, 70 ± 15; 27-30 h, 94.4 ± 2.5) and *CatSperζ*-/- (20 h, 21.3 ± 7.6; 27-30 h, 24.6 ± 7.4). ***P*=0.0097 (One-way ANOVA and F test). See also **Figure 2D**. (D) Sperm motility parameters measured by computer assisted sperm analysis (CASA) from *CatSperζ* het *(+/-*) versus null *(-/-*) male mice. 5 min (basal, gray) and 90 min (capacitated, black) after incubation in HTF. ALH of *CatSperζ*+/- (basal, 15.5 ± 0.4; 120 min, 17.3 ± 0.4, *p*=0.0002). Data are mean ± SEM. N=4. (E) Capacitation-associated protein tyrosine phosphorylation of *CatSperζ* -/- spermatozoa.

Figure 3. $I_{CatSper}$, but not ATP-activated P2X2 current, is Significantly Reduced in *CatSperζ*-null Spermatozoa. (A) *CatSperζ-/-* and (B) CatSper*ζ +/-* $I_{CatSper}$. Left panels show the current-voltage relations of monovalent $I_{CatSper}$ in response to voltage ramps at the time points indicated. Right traces are representative time courses of $I_{CatSper}$ measured in the standard bath solution (1, HS), ATP-activated P2X2 current (2, ATP), and nominally divalent-free solution (3, DVF) at -100 mV (gray circles) and + 100 mV (black circles). $I_{CatSper}$ in *CatSperζ*-null sperm cells is ~60% of that recorded from wt. Inward I_{ATP} current induced by 100 μM ATP is similar in both phenotypes and indistinguishable from previously published wt I_{ATP} (Navarro et al., 2011). (C) Average $I_{CatSper}$ measured from *CatSperζ+/-* (-683 ± 77 pA) and CatSper*ζ-/-* (-426 ± 50 pA) sperm cells at -100 mV. Data are mean ± SEM. *P* = 0.0297. Cartoon shows the standard pipette solution (mM); internal Cs used to block K^+ currents.

Figure 4. CatSper Proteins Are Reduced in Sperm from *CatSperζ*-null Mice despite Protein Expression during Spermatogenesis. (A and B) Reduced expression of CatSper subunits in sperm cells of *CatSperζ* homozygous null mice compared with their complete absence in *CatSper1* and *δ*-null mice. Immunoblotting of (A) total mouse sperm extracts and (B) protein expression ratio (*ζ*-KO/wt) of CatSper 1 (0.5 ± 0.1), 3 (0.6 ± 0.08), 4 (0.3 ± 0.07), β (0.4 ± 0.1), δ (0.4 ± 0.07), and ε (0.5 ± 0.03). Data are mean ±

SEM. (C) Increased expression of CatSper1 and ε in mouse testis in *CatSperζ*-null mutants. (D) Quantitative gene expression analysis (qRT-PCR) from adult *CatSperζ*-het and null testes: expression ratio (2^{-ddCT}) and mean ddCt (null-het); TATA binding protein (TBP) is the internal control. Expression ratio of *CatSper1* (1.1 ± 0.1) and all accessory γ (1.0 ± 0.2), β (1.3 ± 0.07), δ (1.1 ± 0.08), and ε (0.95 ± 0.07) subunits are mean ± SEM.

Figure 5. *CatSperζ* Deletion Disrupts the Continuity of the CatSper Linear Domains. Application of different modes of fluorescence microscopy to observe CatSper localization. (A) Deconvolved confocal image of α-CatSper1 immunostained *CatSperζ*-null spermatozoa. Scale bar, 1 μm. (B and C) 3D super-resolution images of CatSper1. 3D STED (B) and 3D STORM (C) images of *CatSperζ*-null (top) and wt (bottom) sperm flagella, respectively. *x-y* projection colors encode the relative distance from the focal plane along the *z* axis. Scale bar, 500 nm. Arrowheads indicate the junction between the mid-piece and the principal piece (annulus) of the tail. 3D STORM, *y-z* cross-section images are shown on the right. Scale bar, 200 nm. See also **Figure 5-figure supplement 1**.

Figure 5-figure supplement 1. Subcellular Distribution of Immunolocalized CatSper Proteins; Related to Figure 5. (A and B) Angular distributions (left) and profiles (right) of the surface-localized molecules of CatSper1 in *CatSperζ*-het (A) and *CatSperζ*-/- spermatozoa (B) of **Figure 5**. (C and D) Averaged autocorrelation functions along the longitudinal axis (x-axis shown in E, inset) calculated from multiple CatSper domains in *wt* (C) and *CatSperζ*-/- (D) spermatozoa. (n= 8). The longitudinal axis (x) is placed at the flagellar center and the origin at the annulus. (E and F) Fourier transformation of the 1D localization distribution shown in (A) and (B), showing a fundamental frequency of $(800\ nm)^{-1}$ in *CatSperζ*-/- spermatozoa. (E, inset) Cartoon of cylindrical coordinate system for defining the radius and angles of molecular coordinates in STORM images.

Figure 6. *CatSperζ*-null Sperm Rheotax Poorly Due to Low Torque. (A) In-capillary sperm rheotaxis. Rheotactic ability is reduced in sperm lacking *CatSperζ* at all flow rates tested (12-65 μm/s). (B) Rheotactic sperm cells are expressed as the % of total motile spermatozoa counted from 9 s-movies (*CatSperζ*+/-, n=32; *CatSperζ*-/-, n=24). Data are expressed in scatter plots; mean ± SEM (colored bars) of *CatSperζ*+/- (88 ± 2) and *CatSperζ*-/- (24 ± 4) as well as median with interquartile ranges (black boxes) of *CatSperζ*+/- (96, IQR 78-100) and *CatSperζ*-/- (22.5, IQR 0-40). ****$P < 0.0001$. (C) Trajectory of free-swimming sperm in 0.3% methyl cellulose. Movies were taken at 50 fps to compare *CatSperζ*+/- (left) and *CatSperζ*-/- (right) sperm cells; bottom of glass dish, 37°C, 5 min after incubation in capacitation medium (HTF). Overlays of flagellar traces (20 frames, 2 s movie) are generated by hyperstacking binary images with gray intensity scale; end frame in black. Arrows indicate sperm heads in each trace. (D) Sperm rotation rate from *CatSperζ*+/- (5 min, 2.4 ± 0.2; 90 min, 3.1 ± 0.2, p=0.0064) and *CatSperζ*-/- (5 min, 3.8 ± 0.2; 90 min, 3.4 ± 0.3) males after incubation in HTF. Sperm rotation rate is calculated as previously reported (Miki and Clapham, 2012). Data are mean ± SEM. ****$P < 0.0001$. (E and F) *IVF* with epididymal and/or ejaculated *CatSperζ*+/- and *CatSperζ*-/- spermatozoa. 2-cell stage eggs were counted 24 h after insemination. (E) *IVF* rate with cumulus-intact oocytes from *CatSperζ*+/- (epididymal, 71 ± 6) and *CatSperζ*-/- (epididymal, 0.7 ± 0.7; ejaculate, 20 ± 6, P = 0.0051). (F) *IVF* rate of cumulus-free/ZP-intact eggs with (*CatSperζ*+/-, 80 ± 8; *CatSperζ*-/-, 7 ± 7, P = 0.0005; wt, 78 ± 6) or without (*CatSperζ*+/-, 88 ± 6; *CatSperζ*-/-, 0.8 ± 0.8, P = 0.0002) glutathione-containing (GSH; 2 mM) media. Data are mean ± SEM. See also **Figure 6-figure supplement 1**.

Figure 6-figure supplement 1. CatSper-mediated Ca^{2+} Signaling and Development of the Flagellar Envelope; Related to Figure 6. (A) In-capillary sperm rheotaxis. Number of rheotactic sperm cells from each 9 s movie at all flow rates in the range of 12-65 μm/s; from **Figure 6A**. Data are expressed as a

scatter plot with mean ± SEM (colored bars) from *CatSperζ*+/- (7.1 ± 0.6) and *CatSperζ*-/- (1.1 ± 0.2). (B) Working model illustrating the integrity of CatSper Ca^{2+} signaling domains and their relation to flagellar envelopes during sperm rotation. In wt spermatozoa, the CatSper channel forms 4 linear continuous Ca^{2+} signaling domains confined to the principal piece of the flagella. Ca^{2+} entry through the CatSper channels potentiates sperm rotation during capacitation (Miki and Clapham, 2013). With the resulting increased asymmetry and change in wave amplitude, the flagellar envelope is mapped out as a 3-dimensional cone in space, orienting sperm into the flow. Deficits in $I_{CatSper}$ and loss of the continuity of the linear domains in *CatSperζ*-/- null spermatozoa compromise Ca^{2+} signaling and result in rigidity in the proximal region. The inflexibility of *ζ*-/- null spermatozoa from midpiece to halfway through the principal piece constrains the flagellar envelope to a narrower, rod like spatial map. The still active distal tail rotation then drives the more static rod-like structure. This causes the sperm to rotate faster but with less torque, thereby inefficiently orienting them into the flow and yielding less force in orthogonal directions needed to push aside the cumulus cells. (C and D) Flagellar waveform traces of spermatozoa. Movies recorded at 200 fps: *CatSperζ*+/- (top) and *CatSperζ*-/- (bottom) sperm cells tethered on glass coverslips. Overlays of flagellar traces from two beat cycles are generated by hyperstacking binary images; time coded in color. (C) Spermatozoa capacitated under low (0.5, 0.1 mM) or high (4 mM) extracellular calcium. (D) Sperm motility after Ca^{2+} transients by A23187 treatment followed by incubation under capacitation conditions.

Supplemental movie captions

Movie S1. Movement of Free Swimming *CatSperζ+/-* and *-/-* Spermatozoa; Related to Figure 2. Uncapacitated (left) and 90 min capacitated (right) spermatozoa were allowed to disperse for 10 min pre-incubation in a 37°C chamber containing HEPES-HTF; free swimming sperm cells recorded within the next 5 min; video rate 20 fps (1/5 speed), 1 s movies; head trace to track swimming trajectory. (A) *CatSperζ+/-* and (B) *CatSperζ-/-* spermatozoa.

Movie S2. Motility of Tethered *CatSperζ+/-* and *-/-* Spermatozoa; Uncapacitated, Related to Figure 2. Uncapacitated epididymal spermatozoa in non-capacitating M2 media were tethered to the fibronectin-coated glass bottom dish; sperm motility was recorded at 37°C; video rate 200 fps, 2 s movies. (A) *CatSperζ+/-* and (B) *CatSperζ-/-* spermatozoa.

Movie S3. Motility of Tethered *CatSperζ+/-* and *-/-* Spermatozoa; 90 min Capacitated, Related to Figure 2. After 90 min incubation in HTF, capacitated epididymal spermatozoa were tethered to a fibronectin-coated glass bottom dish; sperm motility was recorded at 37°C; video rate 100 fps (1/2 speed), 1 s movies. (A) *CatSperζ+/-* and (B) *CatSperζ-/-* spermatozoa.

Movie S4. In-capillary Rheotaxis of *CatSperζ+/-* and *-/-* Spermatozoa; Capacitated, Related to Figure6. Capacitated epididymal spermatozoa in HTF for 90 min were loaded into the capillary and transferred to a 37°C chamber; sperm cells swimming against the flow and down were recorded; video rate 33 fps, 9 s movies. (A) *CatSperζ+/-* and (B) *CatSperζ-/-* spermatozoa.

Movie S5. Movement of *CatSperζ+/-* and *-/-* Sperm in Viscous Medium; Uncapacitated, Related to Figure 6. Uncapacitated spermatozoa were allowed to disperse for 10 min pre-incubation in a 37°C chamber containing HEPES-HTF supplemented with 0.3% methylcellulose; swimming sperm cells were recorded within the next 5 min; video rate 50 fps, 2 s movies. (A) *CatSperζ+/-* and (B) *CatSperζ-/-* spermatozoa.

Movie S6. Movement of *CatSperζ+/-* and *-/-* Sperm in Viscous Medium; 90 min Capacitated, Related to Figure 6. Spermatozoa capacitated in HTF were allowed to disperse for 10 min pre-incubation in a 37°C chamber containing HEPES-HTF supplemented with 0.3% (left), 0.4% (middle), or 0.5% (right) methylcellulose; swimming sperm cells were recorded within the next 5 min; video rate 50 fps, 2 s movies. (A) *CatSperζ+/-* and (B) *CatSperζ-/-* spermatozoa.

Movie S7. Motility of Tethered *CatSperζ+/-* Sperm in Low External Calcium; 90 min Capacitated, Related to Figure 6-figure supplement 1. After 90 min incubation in Ca^{2+}-HTF under capacitating conditions, *CatSperζ+/-* spermatozoa were tethered to a fibronectin-coated glass bottom dish; sperm motility was recorded within the next 5 min at 37°C; video rate 100 fps (1/2 speed), 1 s movies. (A) 2 Ca^{2+}-HTF, (B) 0.5 Ca^{2+}-HTF and (C) 0.1 Ca^{2+}-HTF (in mM).

Movie S8. Motility of Tethered *CatSperζ-/-* Sperm in High External Calcium; 90 min Capacitated, Related to Figure 6-figure supplement 1. After 90 min incubation in Ca^{2+}-HTF under capacitating conditions, *CatSperζ-/-* spermatozoa were tethered to a fibronectin-coated glass bottom dish; sperm motility was recorded within the next 5 min at 37°C; video rate 100 fps (1/2 speed), 1 s movies. (A) 2 Ca^{2+}-HTF and (B) 4 Ca^{2+}-HTF (in mM).

Movie S9. Motility of Tethered *CatSperζ+/-* and *-/-* Sperm after A23187 Treatment; 5 min after Wash, Related to Figure 6-figure supplement 1. Spermatozoa treated with 20 μM A23187 in H-HTF for 10 min were washed and incubated in HTF under capacitating conditions for 5 min; sperm were tethered to a fibronectin-coated glass bottom dish and the motility was recorded in H-HTF within the next 5 min at 37°C; video rate 100 fps (1/2 speed), 1 s movies. (A) *CatSperζ+/-* and (B) *CatSperζ-/-* spermatozoa.

Movie S10. Motility of Tethered *CatSperζ+/-* and *-/-* Sperm after A23187 Treatment; 30 min after Wash, Related to Figure 6-figure supplement 1. Spermatozoa treated with 20 μM A23187 in H-HTF for 10 min were washed and incubated in HTF under capacitating conditions for 30 min; sperm were tethered to a fibronectin-coated glass bottom dish and the motility was recorded in H-HTF within the next 5 min at 37°C; video rate 100 fps (1/2 speed), 1 s movies. (A) *CatSperζ+/-* and (B) *CatSperζ-/-* spermatozoa.

Source data

Figure 1-figure supplement 2-source data 1. Temporal expression of *CatSper1*, *CatSperε*, and *CatSperζ* mRNAs during postnatal testis development.

Figure 2-source data 1. Impaired male fertility in *CatSperζ-/-* mice: pregnancy rate, litter size, sperm number per egg, and *in vivo* fertilization rate.

Figure 2-figure supplement 2-source data 1. Impaired male fertility in *CatSperζ-/-* mice: sperm count, litter size per genotype, *in vivo* fertilization rate, and CASA parameters.

Figure 3-source data 1. Inward CatSper current at -100 mV.

Figure 4-source data 1. Protein and mRNA expression of CatSper subunits.

Figure 6- source data 1. In-capillary sperm rheotaxis and *in vitro* fertilization.

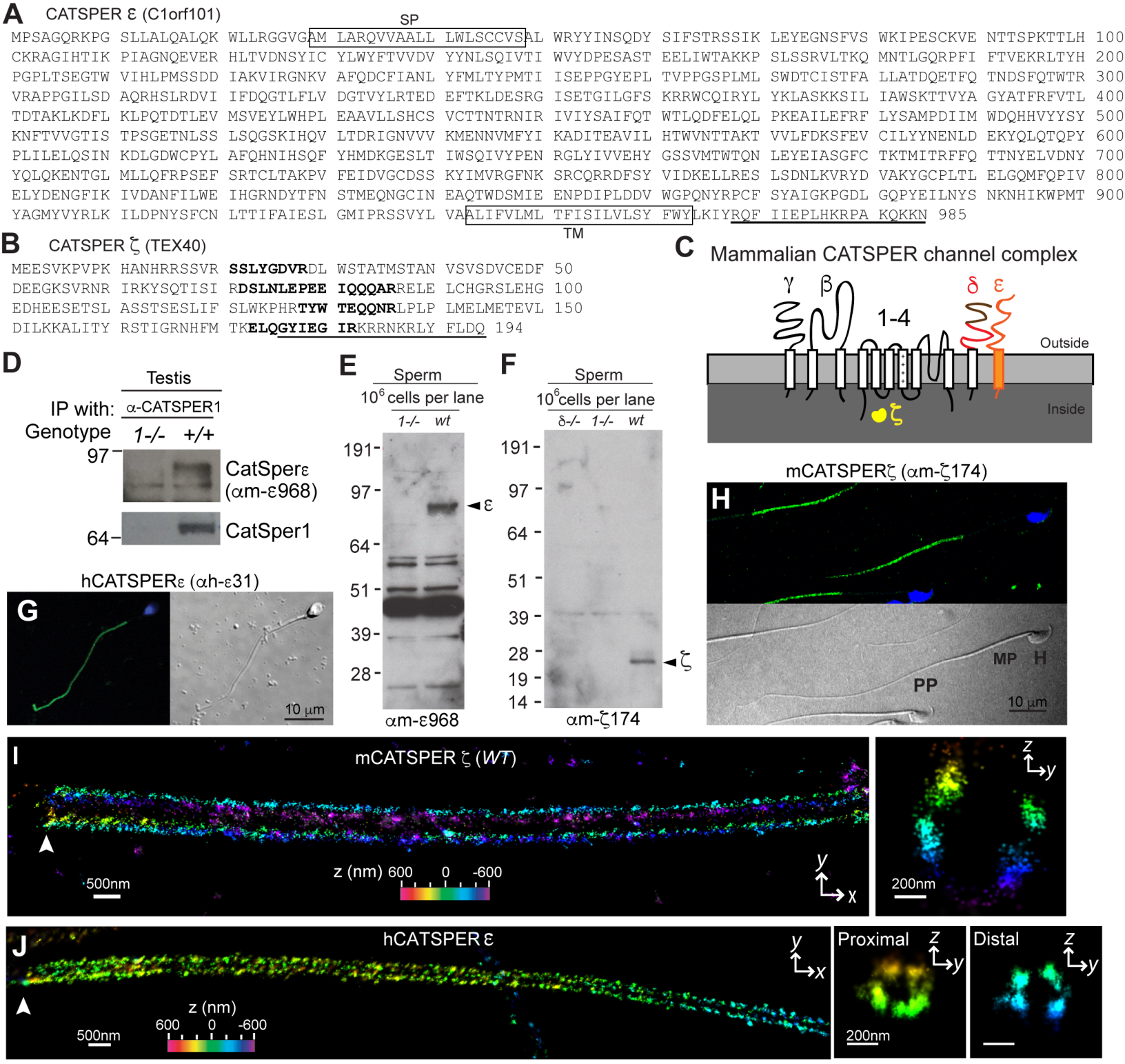
A
CATSPER ε (C1orf101)
SP
MPSAGQRKPG SLLALQALQK WLLRGGVGAM LARQVVAALL LWLSCCVSAL WRYYINSQDY SIFSTRSSIK LEYEGNSFVS WKIPESCKVE NTTSPKTTLH 100
CKRAGIHTIK PIAGNQEVER HLTVDNSYIC YLWYFTVVDV YYNLSQIVTI WVYDPESAST EELIWTAKKP SLSSRVLTKQ MNTLGQRPFI FTVEKRLTYH 200
PGPLTSEGTW VIHLPMSSDD IAKVIRGNKV AFQDCFIANL YFMLTYPMTI ISEPPGYEPL TVPPGSPLML SWDTCISTFA LLATDQETFQ TNDSFQTWTR 300
VRAPPGILSD AQRHSLRDVI IFDQGTLFLV DGTVYLRTED EFTKLDESRG ISETGILGFS KRRWCQIRYL YKLASKKSIL IAWSKTTVYA GYATFRFVTL 400
TDTAKLKDFL KLPQTDTLEV MSVEYLWHPL EAAVLLSHCS VCTTNTRNIR IVIYSAIFQT WTLQDFELQL PKEAILEFRF LYSAMPDIIM WDQHHVYYSY 500
KNFTVVGTIS TPSGETNLSS LSQGSKIHQV LTDRIGNVVV KMENNVMFYI KADITEAVIL HTWVNTTAKT VVLFDKSFEV CILYYNENLD EKYQLQTQPY 600
PLILELQSIN KDLGDWCPYL AFQHNIHSQF YHMDKGESLT IWSQIVYPEN RGLYIVVEHY GSSVMTWTQN LEYEIASGFC TKTMITRFFQ TTNYELVDNY 700
YQLQKENTGL MLLQFRPSEF SRTCLTAKPV FEIDVGCDSS KYIMVRGFNK SRCQRRDFSY VIDKELLRES LSDNLKVRYD VAKYGCPLTL ELGQMFQPIV 800
ELYDENGFIK IVDANFILWE IHGRNDYTFN STMEQNGCIN EAQTWDSMIE ENPDIPLDDV WGPQNYRPCF SYAIGKPGDL GQPYEILNYS NKNHIKWPMT 900
YAGMYVYRLK ILDPNYSFCN LTTIFAIESL GMIPRSSVYL VAALIFVLML TFISILVLSY FWYLKIYRQF IIEPLHKRPA KQKKN 985
TM
B
CATSPER ζ (TEX40)
MEESVKPVPK HANHRRSSVR SSLYGDVRDL WSTATMSTAN VSVSDVCEDF 50
DEEGKSVRNR IRKYSQTISI RDSLNLEPEE IQQQARRELE LCHGRSLEHG 100
EDHEESETSL ASSTSESLIF SLWKPHRTYW TEQQNRLPLP LMELMETEVL 150
DILKKALITY RSTIGRNHFM TKELQGYIEG IRKRRNKRLY FLDQ 194
C
Mammalian CATSPER channel complex
γ
β
1-4
δ
ε
Outside
Inside
ζ
D
Testis
IP with: α-CATSPER1
Genotype 1-/- +/+
97
64
CatSperε (αm-ε968)
CatSper1
E
Sperm
10^6 cells per lane
1-/- wt
191
97
64
51
39
28
ε
αm-ε968
F
Sperm
10^6 cells per lane
δ-/- 1-/- wt
191
97
64
51
39
28
19
14
ζ
αm-ζ174
mCATSPERζ (αm-ζ174)
H
MP
H
PP
10 μm
hCATSPERε (αh-ε31)
G
10 μm
I
mCATSPER ζ (WT)
500nm
z (nm) 600 0 -600
y
x
z
y
200nm
J
hCATSPER ε
500nm
z (nm)
600 0 -600
y
x
Proximal
z
y
200nm
Distal
z
y

Figure 1.

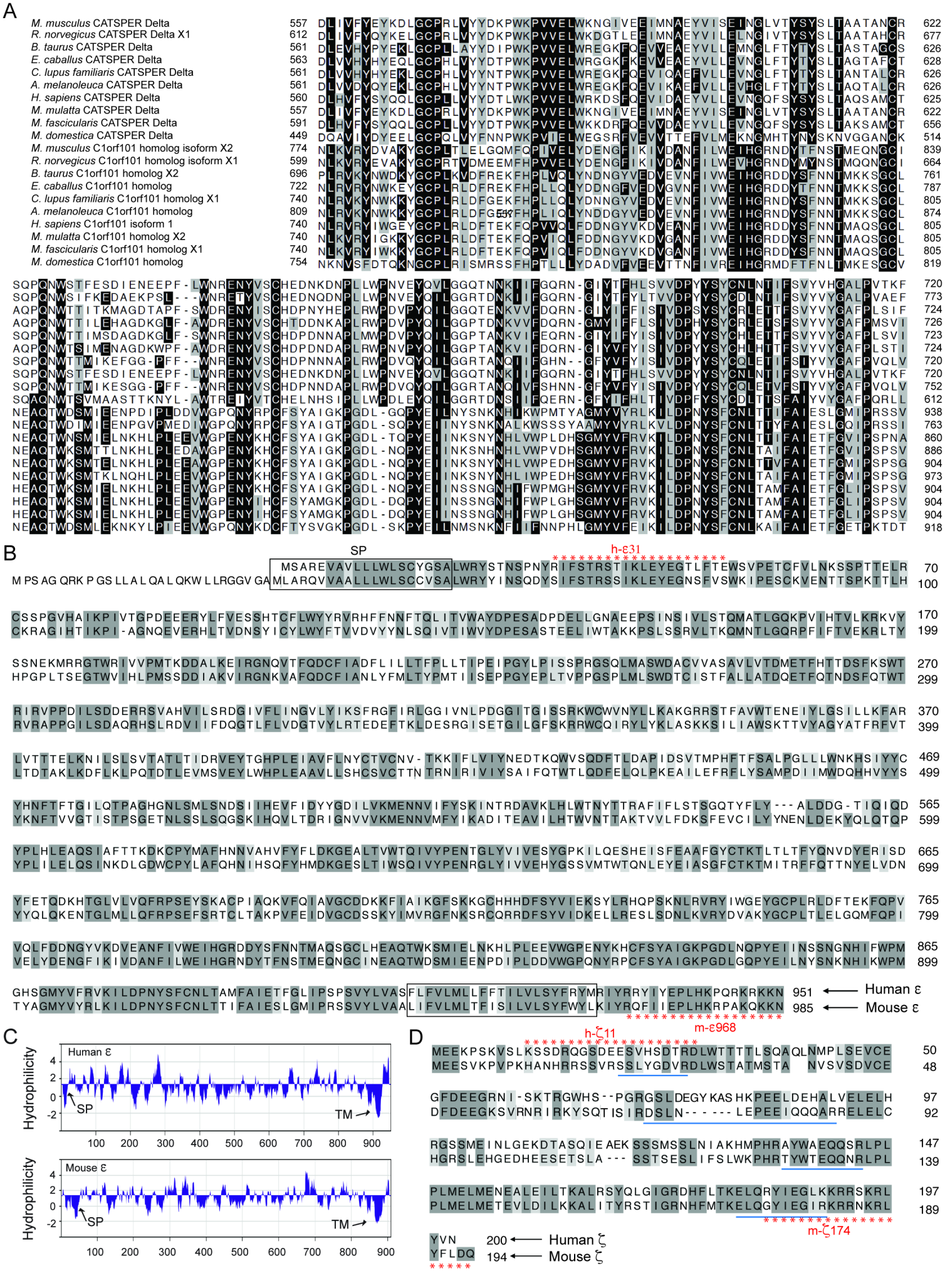
A
M. musculus CATSPER Delta
R. norvegicus CATSPER Delta X1
B. taurus CATSPER Delta
E. caballus CATSPER Delta
C. lupus familiaris CATSPER Delta
A. melanoleuca CATSPER Delta
H. sapiens CATSPER Delta
M. mulatta CATSPER Delta
M. fascicularis CATSPER Delta
M. domestica CATSPER Delta
M. musculus C1orf101 homolog isoform X2
R. norvegicus C1orf101 homolog isoform X1
B. taurus C1orf101 homolog X2
E. caballus C1orf101 homolog
C. lupus familiaris C1orf101 homolog X1
A. melanoleuca C1orf101 homolog
H. sapiens C1orf101 isoform 1
M. mulatta C1orf101 homolog X2
M. fascicularis C1orf101 homolog X1
M. domestica C1orf101 homolog
B
SP
h-ε31
Human ε
Mouse ε
m-ε968
C
Human ε
Mouse ε
Hydrophilicity
SP
TM
D
h-ζ11
m-ζ174
Human ζ
Mouse ζ

Figure S1.

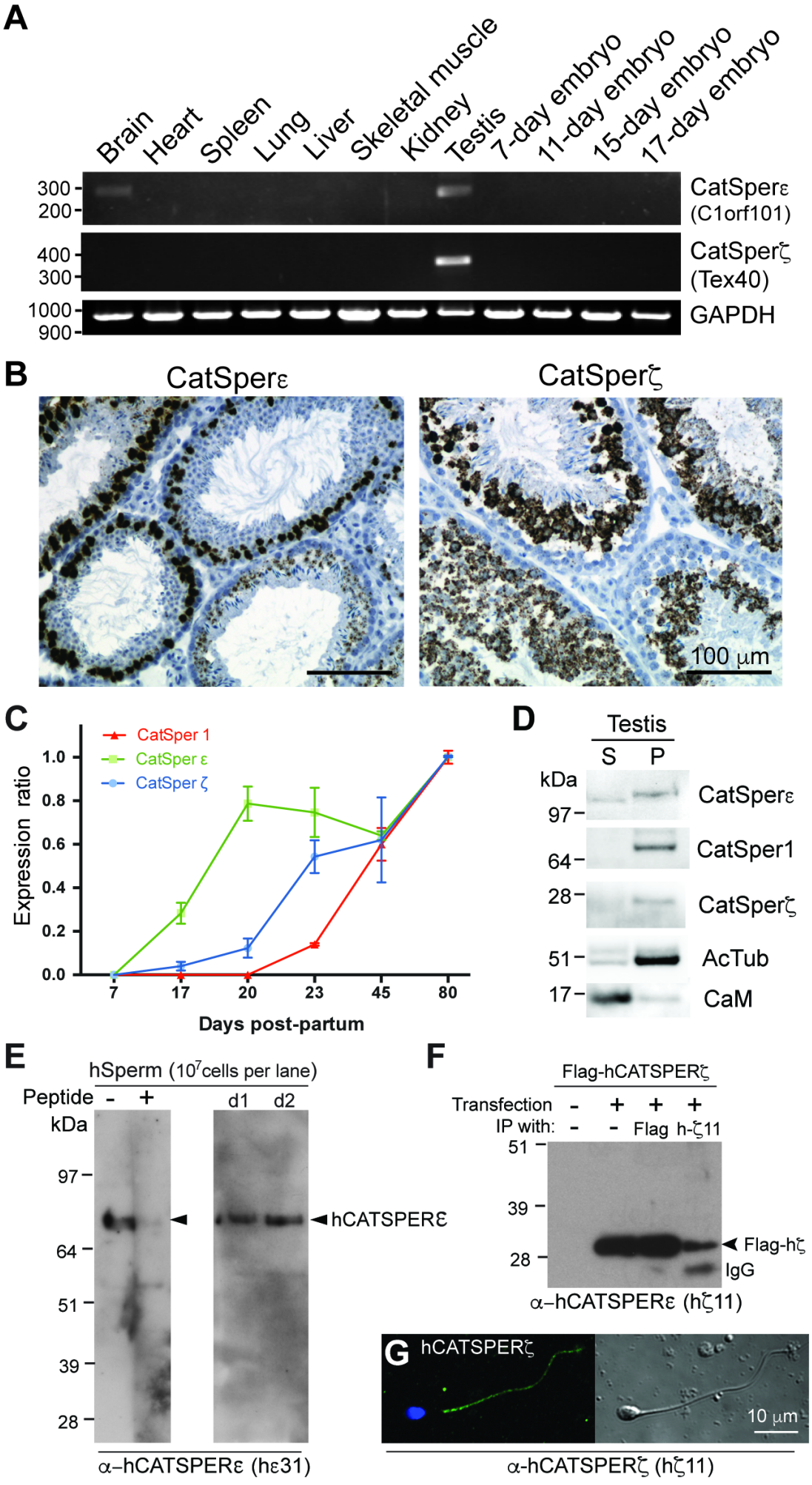
A
Brain
Heart
Spleen
Lung
Liver
Skeletal muscle
Kidney
Testis
7-day embryo
11-day embryo
15-day embryo
17-day embryo
300
200
CatSperε
(C1orf101)
400
300
CatSperζ
(Tex40)
1000
900
GAPDH
B
CatSperε
CatSperζ
100 μm
C
CatSper 1
CatSper ε
CatSper ζ
Expression ratio
1.0
0.8
0.6
0.4
0.2
0.0
7
17
20
23
45
80
Days post-partum
D
Testis
S
P
kDa
97
64
28
51
17
CatSperε
CatSper1
CatSperζ
AcTub
CaM
E
hSperm (10^7cells per lane)
Peptide
-
+
d1
d2
kDa
97
64
51
39
28
hCATSPERε
α–hCATSPERε (hε31)
F
Flag-hCATSPERζ
Transfection
-
+
+
+
IP with:
-
-
Flag
h-ζ11
51
39
28
Flag-hζ
IgG
α–hCATSPERε (hζ11)
G
hCATSPERζ
10 μm
α-hCATSPERζ (hζ11)

Figure S2.

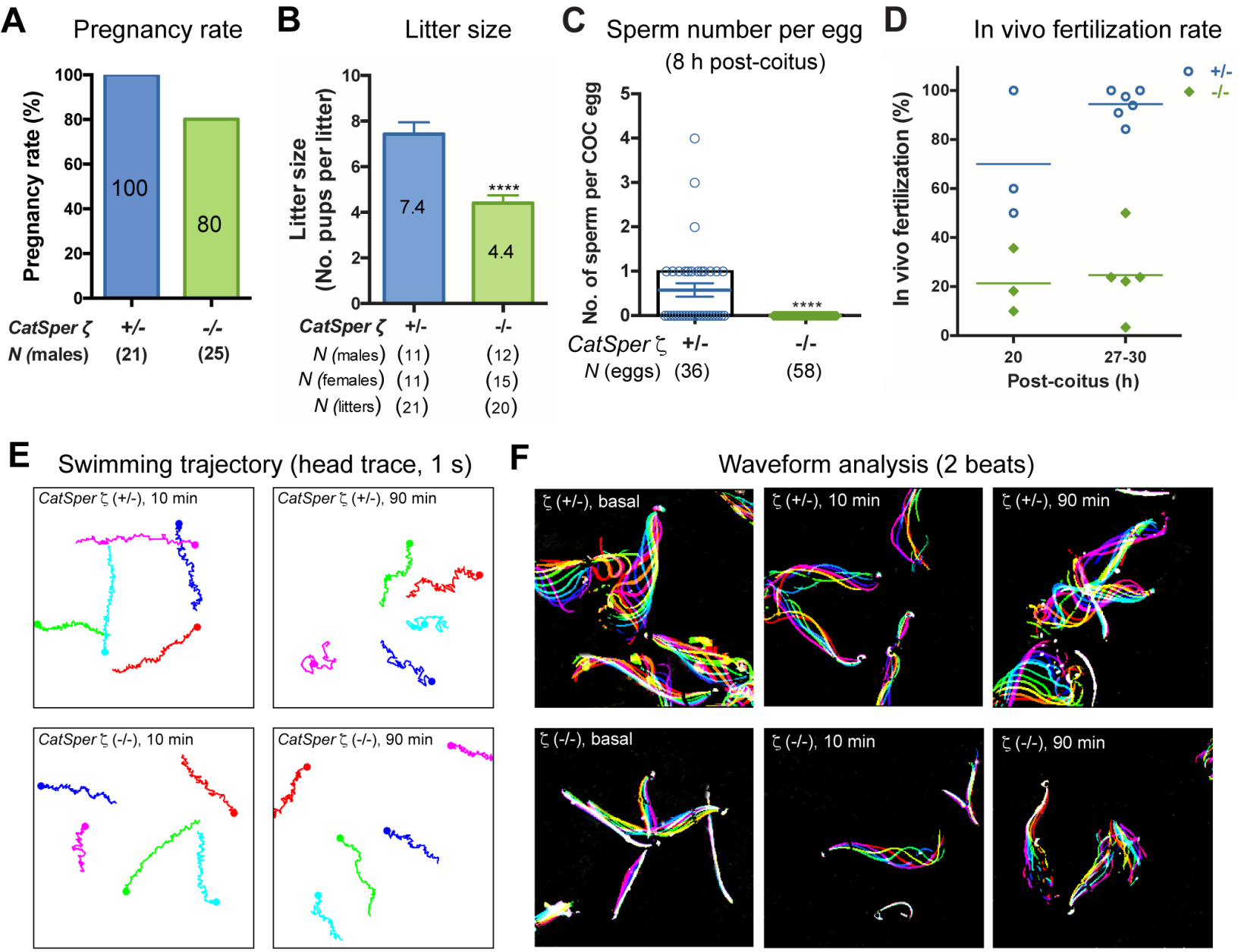
A
Pregnancy rate
Pregnancy rate (%)
100
80
CatSper ζ +/- -/-
N (males) (21) (25)
B
Litter size
Litter size (No. pups per litter)
7.4
4.4
****
CatSper ζ +/- -/-
N (males) (11) (12)
N (females) (11) (15)
N (litters) (21) (20)
C
Sperm number per egg
(8 h post-coitus)
No. of sperm per COC egg
****
CatSper ζ +/- -/-
N (eggs) (36) (58)
D
In vivo fertilization rate
In vivo fertilization (%)
+/-
-/-
20
27-30
Post-coitus (h)
E
Swimming trajectory (head trace, 1 s)
CatSper ζ (+/-), 10 min
CatSper ζ (+/-), 90 min
CatSper ζ (-/-), 10 min
CatSper ζ (-/-), 90 min
F
Waveform analysis (2 beats)
ζ (+/-), basal
ζ (+/-), 10 min
ζ (+/-), 90 min
ζ (-/-), basal
ζ (-/-), 10 min
ζ (-/-), 90 min

Figure 2.

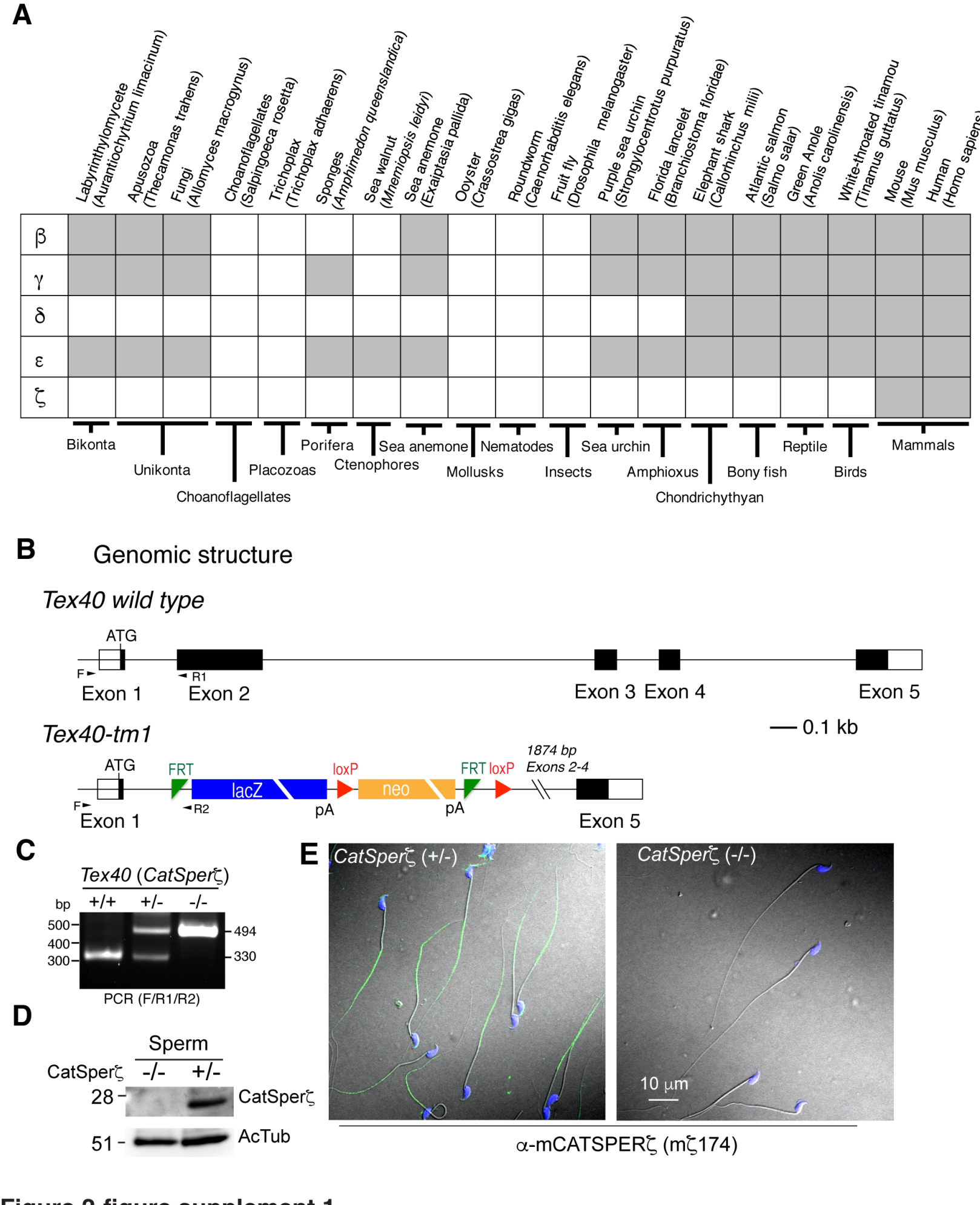

Figure 2-figure supplement 1

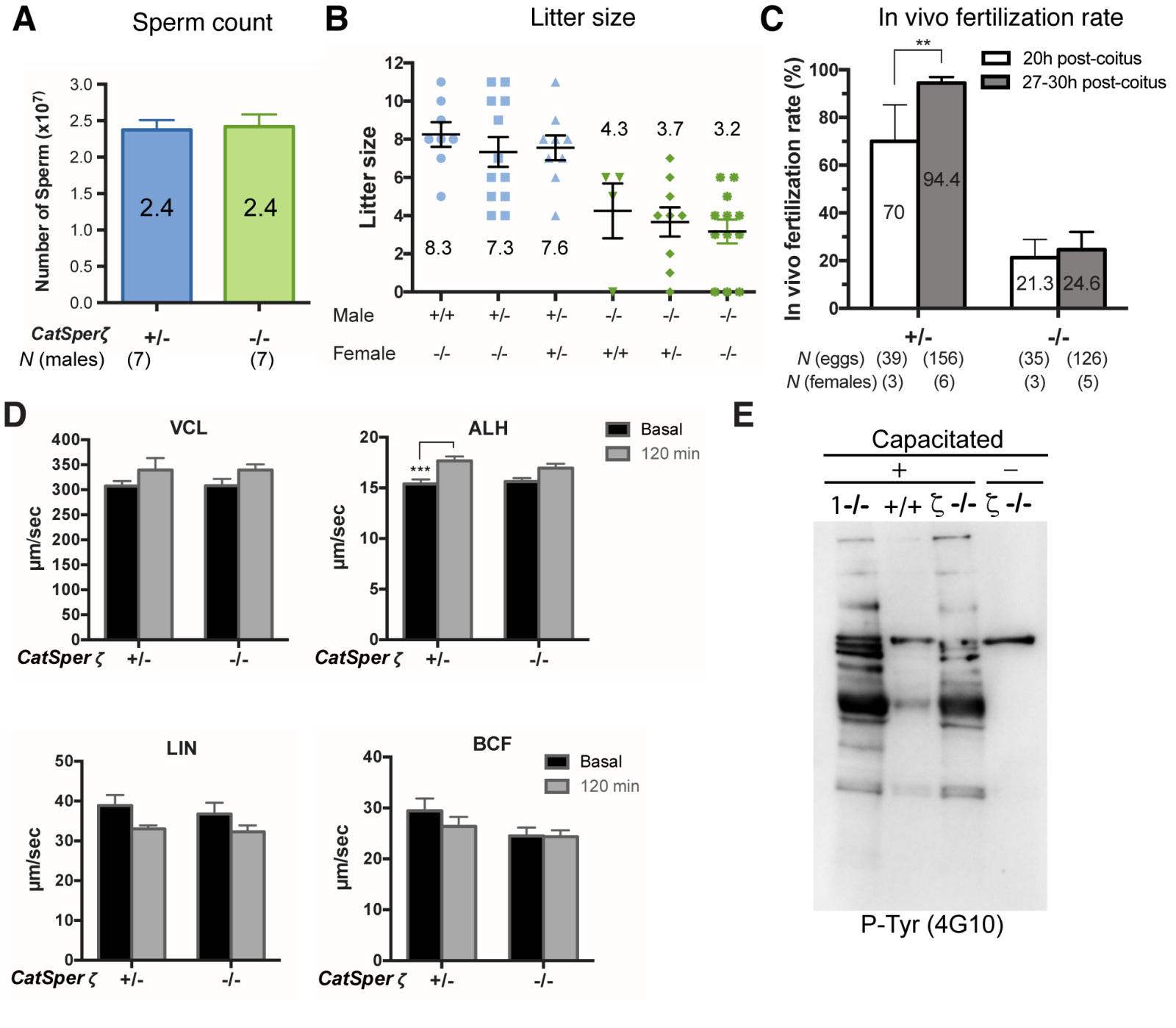
A
Sperm count
Number of Sperm (x10⁷)
3.0
2.5
2.0
1.5
1.0
0.5
0.0
2.4
2.4
CatSperζ +/- -/-
N (males) (7) (7)
B
Litter size
Litter size
12
10
8
6
4
2
0
8.3
7.3
7.6
4.3
3.7
3.2
Male +/+ +/- +/- -/- -/- -/-
Female -/- -/- +/- +/+ +/- -/-
C
In vivo fertilization rate
In vivo fertilization rate (%)
100
80
60
40
20
0
**
20h post-coitus
27-30h post-coitus
70
94.4
21.3
24.6
+/- -/-
N (eggs) (39) (156) (35) (126)
N (females) (3) (6) (3) (5)
D
VCL
ALH
Basal
120 min
µm/sec
400
350
300
250
200
150
100
50
0
20
15
10
5
0
***
CatSperζ +/- -/-
CatSperζ +/- -/-
LIN
BCF
50
40
30
20
10
0
CatSperζ +/- -/-
CatSperζ +/- -/-
E
Capacitated
+
–
1-/- +/+ ζ -/- ζ -/-
P-Tyr (4G10)

Figure S4.

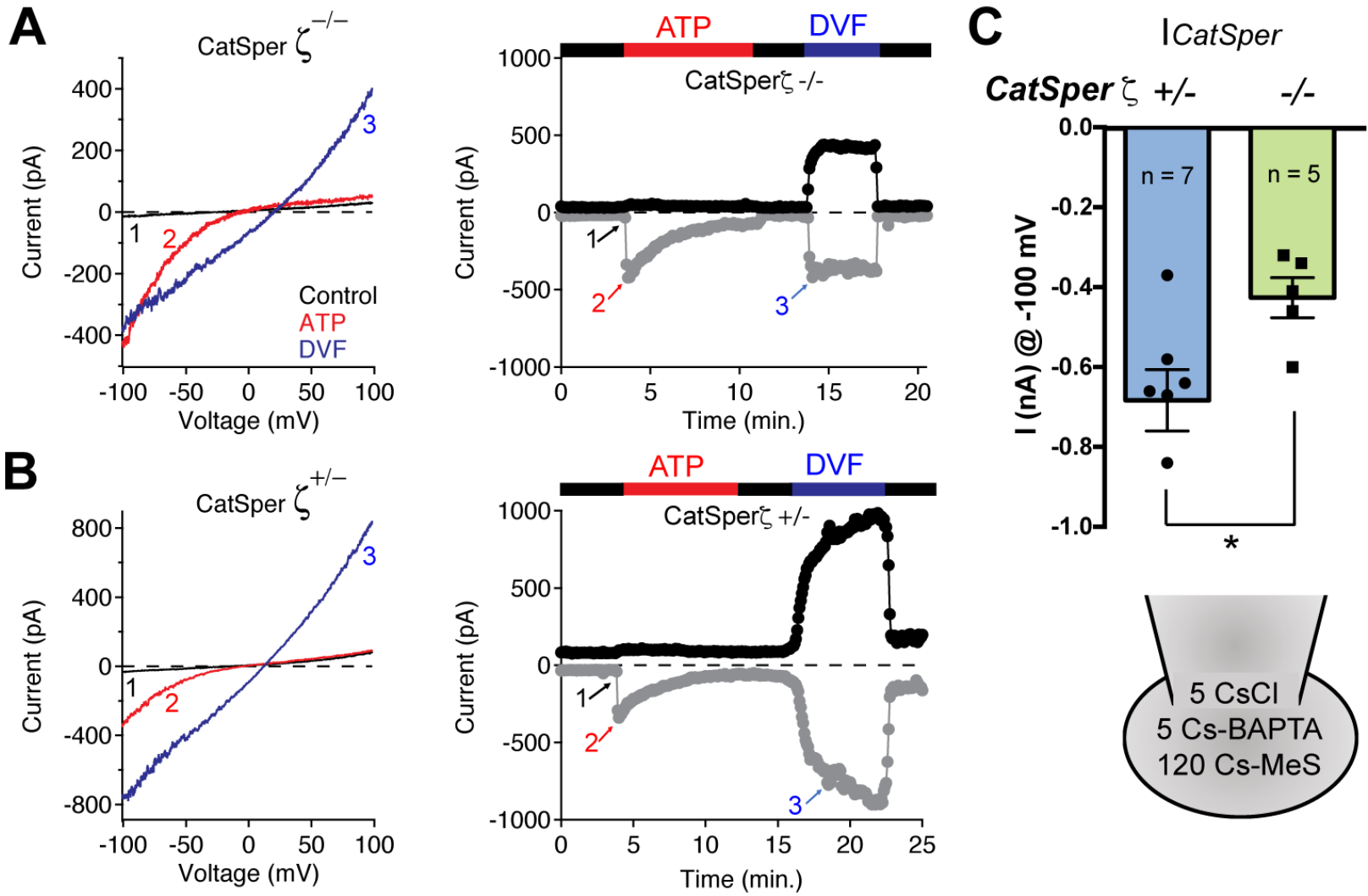
A
CatSper ζ −/−
Current (pA)
Voltage (mV)
Control
ATP
DVF
ATP
DVF
CatSperζ -/-
Time (min.)
B
CatSper ζ +/−
CatSperζ +/-
C
ICatSper
CatSper ζ +/-
-/-
I (nA) @ -100 mV
n = 7
n = 5
*
5 CsCl
5 Cs-BAPTA
120 Cs-MeS

Figure 3

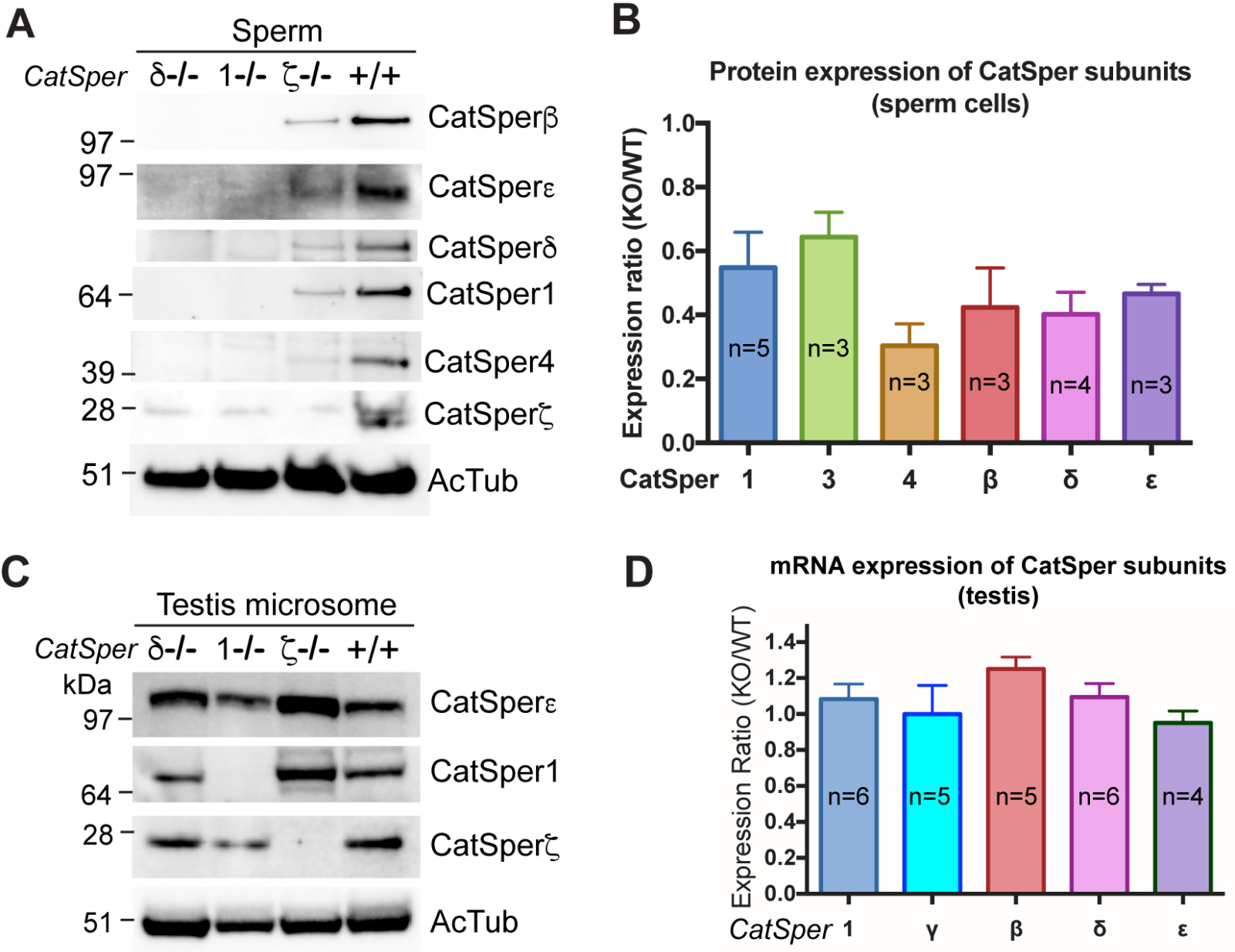
A
Sperm
CatSper δ-/- 1-/- ζ-/- +/+
97
97
64
39
28
51
CatSperβ
CatSperε
CatSperδ
CatSper1
CatSper4
CatSperζ
AcTub
B
Protein expression of CatSper subunits (sperm cells)
Expression ratio (KO/WT)
1.0
0.8
0.6
0.4
0.2
0.0
n=5
n=3
n=3
n=3
n=4
n=3
CatSper 1 3 4 β δ ε
C
Testis microsome
CatSper δ-/- 1-/- ζ-/- +/+
kDa
97
64
28
51
CatSperε
CatSper1
CatSperζ
AcTub
D
mRNA expression of CatSper subunits (testis)
Expression Ratio (KO/WT)
1.4
1.2
1.0
0.8
0.6
0.4
0.2
0.0
n=6
n=5
n=5
n=6
n=4
CatSper 1 γ β δ ε

Figure 4

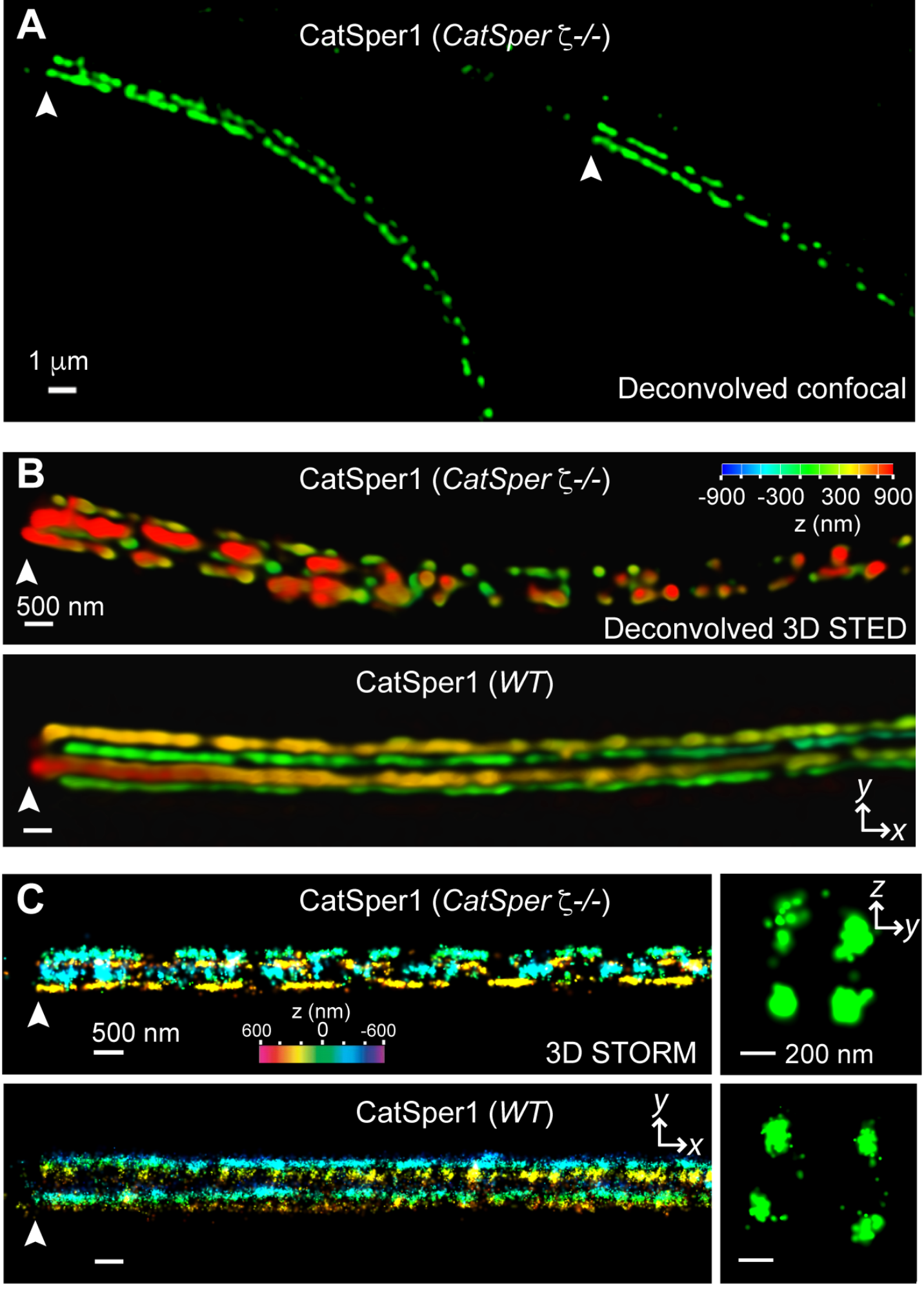
A
CatSper1 (CatSper ζ-/-)
1 μm
Deconvolved confocal
B
CatSper1 (CatSper ζ-/-)
-900 -300 300 900
z (nm)
500 nm
Deconvolved 3D STED
CatSper1 (WT)
y
x
C
CatSper1 (CatSper ζ-/-)
500 nm
z (nm)
600 0 -600
3D STORM
z
y
200 nm
CatSper1 (WT)
y
x

Figure 5

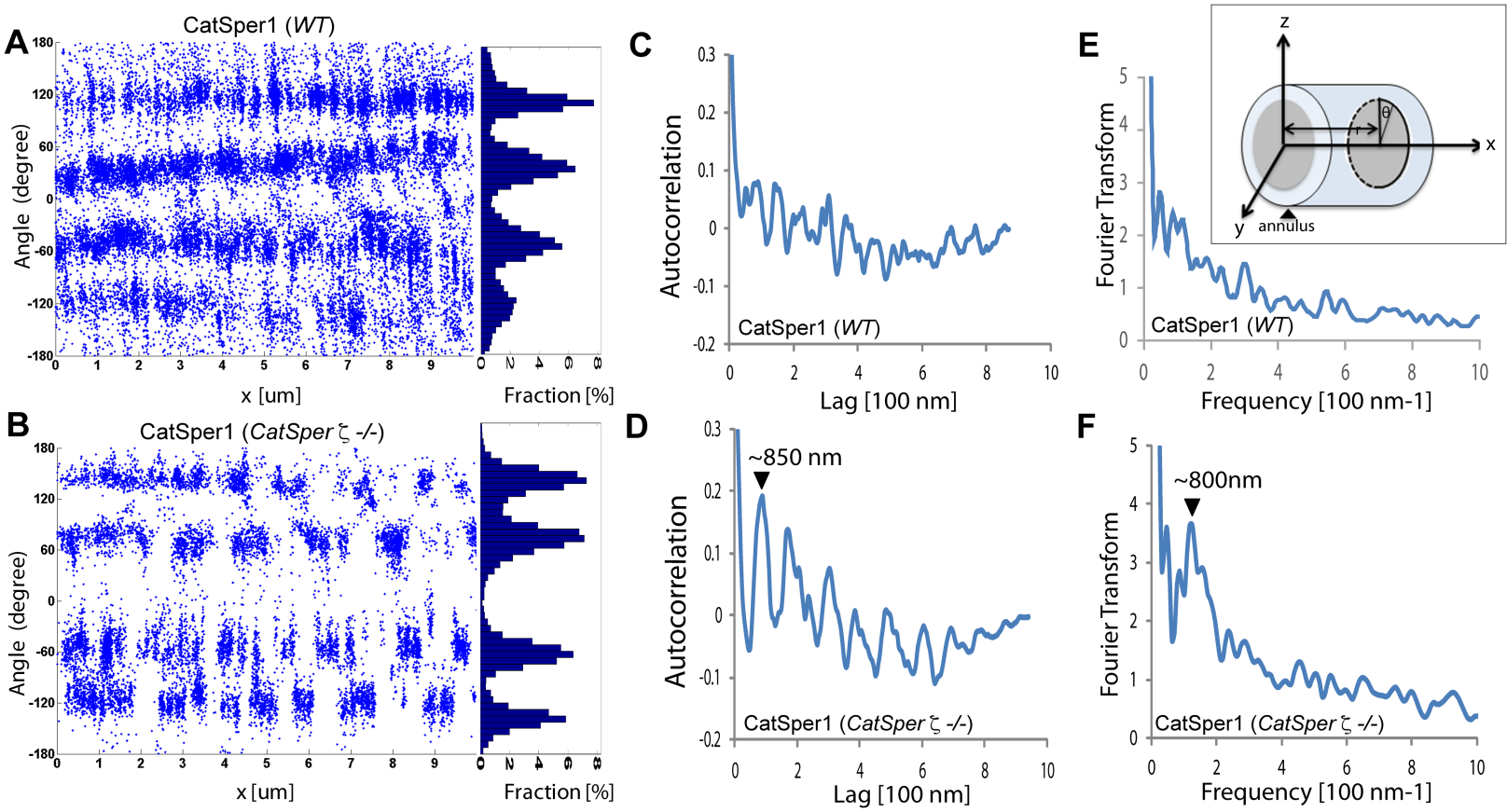

Figure 5-figure supplement 1

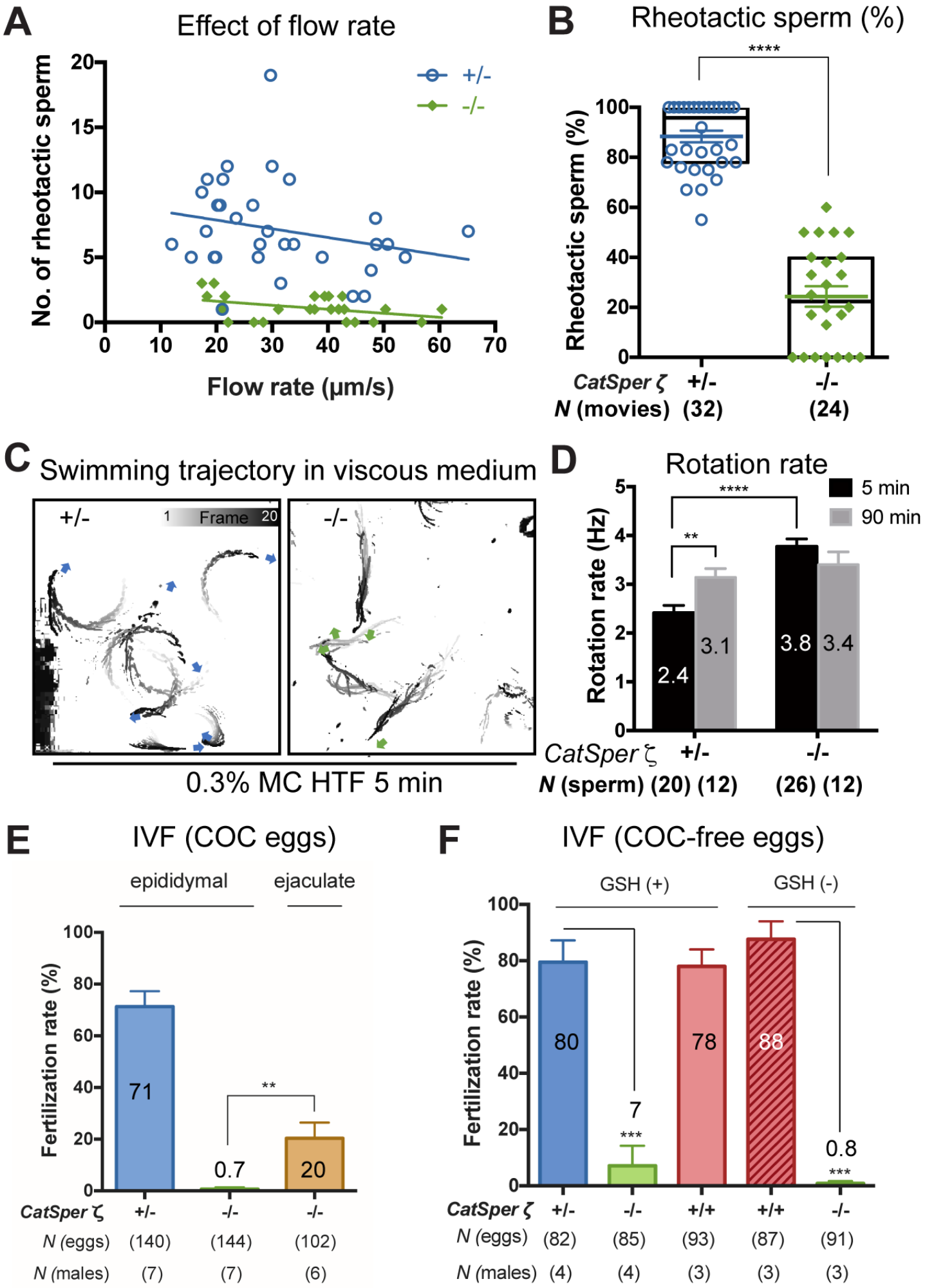
A
Effect of flow rate
No. of rheotactic sperm
Flow rate (μm/s)
+/-
-/-
B
Rheotactic sperm (%)
****
Rheotactic sperm (%)
CatSper ζ +/- -/-
N (movies) (32) (24)
C
Swimming trajectory in viscous medium
+/-
Frame
-/-
0.3% MC HTF 5 min
D
Rotation rate
5 min
90 min
****
**
Rotation rate (Hz)
2.4
3.1
3.8
3.4
CatSper ζ +/- -/-
N (sperm) (20) (12) (26) (12)
E
IVF (COC eggs)
epididymal
ejaculate
Fertilization rate (%)
71
**
0.7
20
CatSper ζ +/- -/- -/-
N (eggs) (140) (144) (102)
N (males) (7) (7) (6)
F
IVF (COC-free eggs)
GSH (+)
GSH (-)
Fertilization rate (%)
80
7
***
78
88
0.8
***
CatSper ζ +/- -/- +/+ +/+ -/-
N (eggs) (82) (85) (93) (87) (91)
N (males) (4) (4) (3) (3) (3)

Figure 6

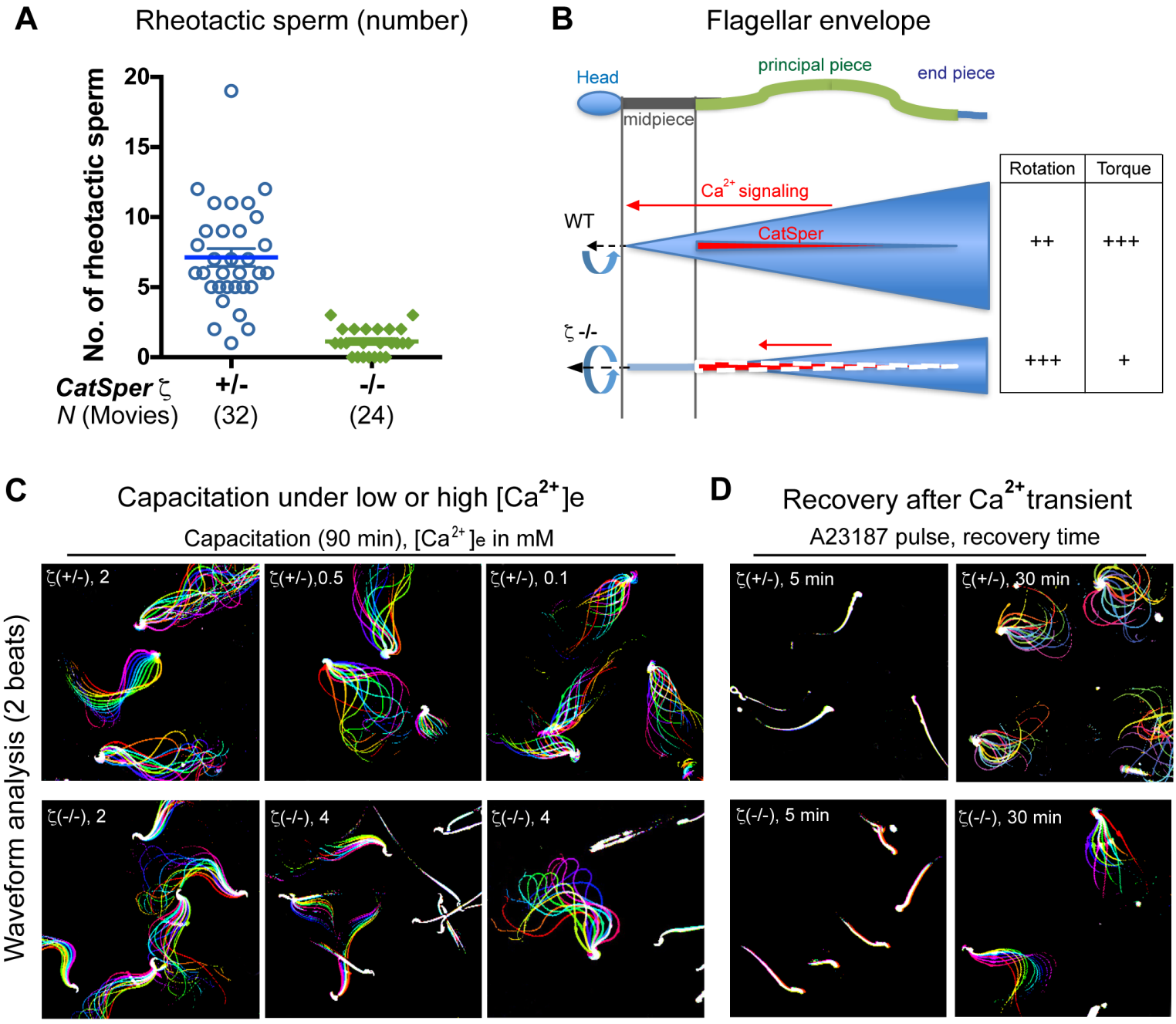

Figure 6-figure supplement 1